Pediatric Ribs at Chest Radiography: Normal Variants and Abnormalities

Yuko Tsujioka, MD • Atsuhiko Handa, MD* • Gen Nishimura, MD, PhD • Taiki Nozaki, MD, PhD • Osamu Miyazaki, MD, PhD*
Tatsuo Kono, MD, PhD • Sarah D. Bixby, MD, MBA • Masahiro Jinzaki, MD, PhD

Author affiliations, funding, and conflicts of interest are listed at the end of this article.
*Y.T. and A.H. contributed equally to this work.

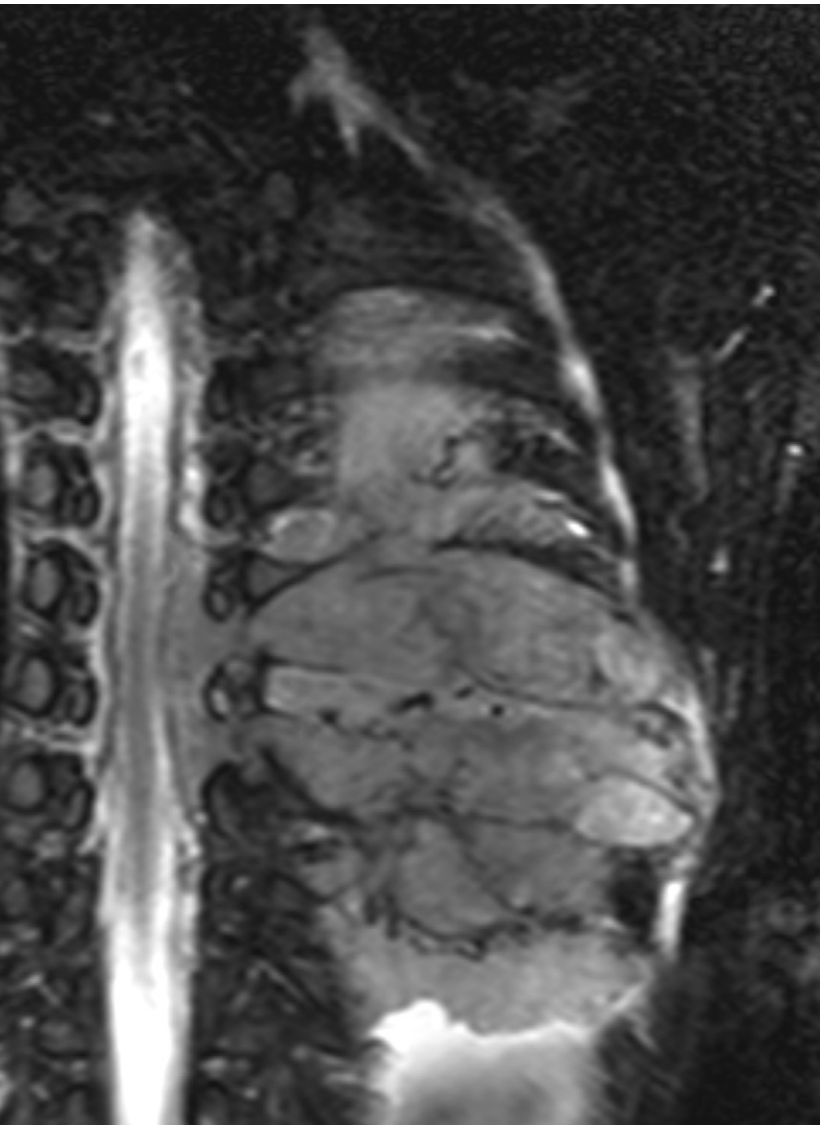

Normal variants and abnormalities of the ribs are frequently encountered on chest radiographs. Accurate identification of normal variants is crucial to avoid unnecessary investigations. A meticulous evaluation of rib abnormalities can provide valuable insights into the patient's symptoms, and even when no osseous condition is suspected, rib abnormalities may offer critical clues to underlying conditions. Rib abnormalities are associated with various conditions, including benign tumors, malignant tumors, infectious and inflammatory conditions, vascular abnormalities, metabolic disorders, nonaccidental injuries, malformation syndromes, and bone dysplasias. Abnormalities of the ribs are classified into three groups based on their radiographic patterns: focal, multifocal, and diffuse changes. Focal lesions are further subdivided into nonaggressive lesions, aggressive lesions, and infectious and inflammatory disorders. Radiologists should be aware of individual disorders of the pediatric ribs, including their imaging findings, relevant clinical information, and underlying pathogenesis. Differential diagnoses are addressed as appropriate. Since chest radiographs can suffice for diagnosis in certain cases, the authors emphasize a pattern recognition approach to radiographic interpretation. However, additional cross-sectional imaging may be necessary for focal lesions such as tumors or inflammatory conditions. Awareness of disease-specific imaging findings helps ascertain the nature of the lesion and directs appropriate management.

Introduction

Rib abnormalities are commonly seen on chest radiographs, although they can be overlooked when cardiopulmonary findings attract the radiologist's attention (known as "satisfaction of search"). Therefore, it is important to carefully examine all chest radiographs for rib abnormalities, as they may explain the patient's symptoms or indicate an underlying condition that has not been diagnosed. Rib abnormalities can be associated with various conditions, including tumors and tumorlike lesions, infectious and inflammatory disorders, metabolic disorders, accidental and nonaccidental injuries, malformation syndromes, and bone dysplasias.

Supplemental Material

Quiz questions for this article are available in the supplemental material.

RadioGraphics 2023; 43(12):e230076
https://doi.org/10.1148/rg.230076

Content Codes: MK, PD

Abbreviations: ABC = aneurysmal bone cyst, CNO = chronic nonbacterial osteomyelitis, LCH = Langerhans cell histiocytosis, NF1 = neurofibromatosis type 1, TSC = tuberous sclerosis complex

TEACHING POINTS

- Rib abnormalities can be associated with various conditions, including tumors and tumorlike lesions, infectious and inflammatory disorders, metabolic disorders, accidental and nonaccidental injuries, malformation syndromes, and bone dysplasias.
- Most tumors or tumorlike conditions tend to occur at the anterior end of the rib (ie, costochondral junction) as it is considered a metaphyseal equivalent of the tubular bones.
- On radiographs, nonaggressive features of rib lesions are similar to those found in the long bones. Lesions are usually geographic (a well-defined margin with or without sclerotic borders), with a narrow zone of transition and a smooth and uniform periosteal reaction without interruption (if present), and without an associated soft-tissue mass.
- Aggressive features of rib lesions on chest radiographs include ill-defined margins with a wide zone of transition, permeative or "moth-eaten" areas of bone destruction, an irregular periosteal reaction, and an associated soft-tissue mass.
- The imaging findings of infectious and inflammatory disorders overlap with those of aggressive bone tumors. Although the findings at clinical presentation usually allow differentiation, biopsy may be warranted to confirm the diagnosis.

In this article, we provide a comprehensive review of pediatric ribs. We first review the normal anatomy of the ribs and benign congenital anomalies that should be accurately identified to avoid unnecessary investigations. We then discuss rib abnormalities that we categorize into three groups based on their radiographic patterns: focal, multifocal, and diffuse rib abnormalities. Within each group, we describe individual disorders and their imaging characteristics, along with relevant clinical and pathogenic findings. In some instances, chest radiographs alone may provide pathognomonic and diagnostic findings. Therefore, we primarily focus on a pattern recognition approach to chest radiograph interpretation. However, cross-sectional imaging such as CT or MRI may be necessary, especially for focal lesions like tumors and inflammatory conditions. Corresponding cross-sectional images are also included in this article where appropriate.

Embryonal Development and Normal Anatomy of the Ribs

Twelve paired ribs are arc-shaped bones that form the thoracic cage (1). The ribs belong to the axial skeleton that stems from the sclerotome (2). The fundamental form (primordium) of the rib derives from the costal (transverse) process of each thoracic vertebra. The rib is a segmental bone consisting of the posterior segment, posterolateral arc, and anterolateral arc. Each of these three segments is controlled by different genes during development (3). The ribs develop via the process of endochondral ossification in which a cartilaginous model or template of the ribs is converted into bone tissue through a series of steps. The anterior end of the rib remains cartilaginous throughout life. The posterior end of the ribs connects to the vertebral column via the costovertebral and costotransverse joints. The upper seven ribs attach to the sternum via the costal cartilage, while the eighth through 10th ribs do not directly articulate with the sternum but instead connect to the costal cartilage of the seventh rib (4). The 11th and 12th ribs are not connected to the costal cartilage and thus are considered floating. The alignment of the ribs changes with age. The anterior ribs are horizontal in the neonatal period, while they are directed downward in childhood.

Congenital Anomalies of the Ribs

Isolated congenital rib anomalies, including variants of the ribs in terms of shape, position, and number, are common and regarded as benign normal variants (Table 1). Bifid (forked) rib and bridging (fused) rib are common developmental anomalies caused by malsegmentation. These variants are usually asymptomatic but may occasionally manifest as a palpable chest wall mass. US may be requested before chest radiography, and either US or chest radiography may confirm the causative rib anomaly (Fig 1).

Anomalous development of the sternocostal junction causes common developmental variants of the thoracic cage such as pectus excavatum and pectus carinatum. Abnormal rib development also alters rib alignment, for example, by causing the anterior ribs to be vertical with pectus excavatum.

The cervical rib is a supernumerary rib arising from the seventh cervical vertebra (Fig 2). This common anomaly is usually asymptomatic in childhood, but it may cause thoracic outlet syndrome and lead to nerve and/or vascular compression that typically manifests in adolescence and adulthood. The intrathoracic rib (Fig 3) is an extra rib that arises either from a vertebra or posterior portion of a rib and extends inferiorly. However, it may occur in any direction. Intrathoracic ribs may be rarely seen surrounded by a parietal and/or visceral pleural sheath. Missing ribs or 11 paired ribs can be seen in normal individuals, although this anomaly occurs in one-third of patients with trisomy 21 syndrome (1).

Since the primordium of the rib derives from the costal (transverse) process of each thoracic vertebra, spinal segmentation anomalies can be accompanied by rib malformations, which may be a component of malformation syndromes. A combination of multiple rib and vertebral anomalies, particularly costovertebral malsegmentation, is associated with certain syndromes (eg, Gorlin-Goltz syndrome, Robinow syndrome, and spondylothoracic dysplasia). However, note that isolated rib anomalies are more common because embryologic development of the rib is independent of that of the vertebra after it derives from the costal process.

Focal Rib Abnormalities

Focal lesions (eg, tumorous and inflammatory lesions) that occur in the appendicular skeleton can involve the ribs as well (Table 2). Most tumors or tumorlike conditions tend to occur at the anterior end of the rib (ie, costochondral junction) as it is considered a metaphyseal equivalent of the tubular bones. The Ewing sarcoma family of tumors is an exception to this pattern, as they have a predilection for affecting the middle

Table 1: Benign Congenital Anomalies of the Ribs (Normal Variants)

Entity	Imaging Findings
Bifid (forked) rib	Forklike deformity of the anterior end
Bridging (fused) rib	Bone or osteocartilaginous bridge of adjoining ribs
Cervical rib	Supernumerary rib arising from the C7 vertebra
Intrathoracic rib	Supernumerary rib with unusual orientation in the thorax

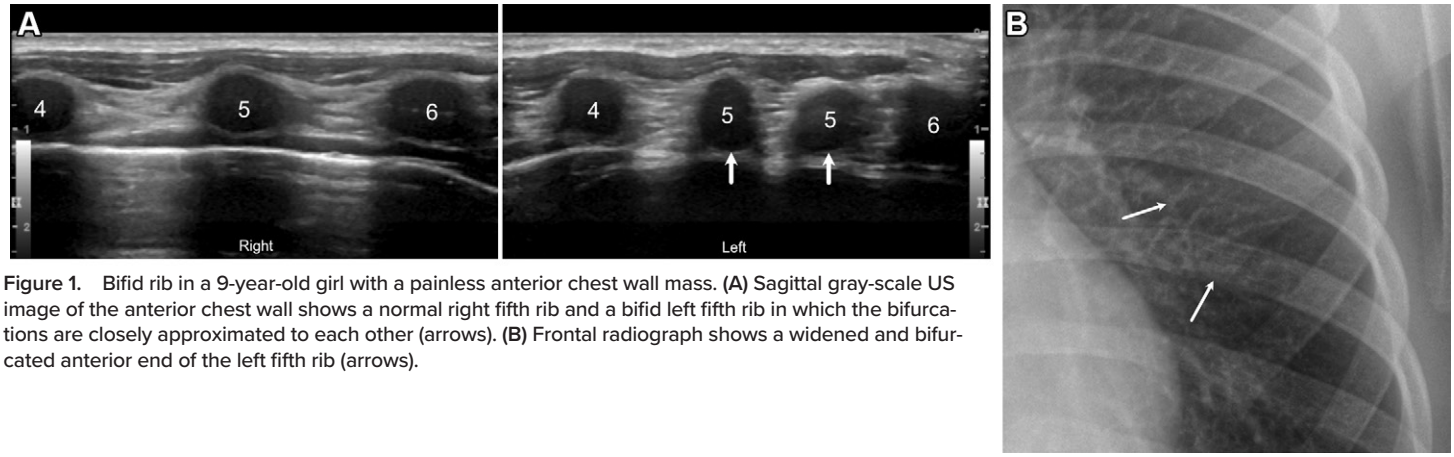

Figure 1. Bifid rib in a 9-year-old girl with a painless anterior chest wall mass. **(A)** Sagittal gray-scale US image of the anterior chest wall shows a normal right fifth rib and a bifid left fifth rib in which the bifurcations are closely approximated to each other (arrows). **(B)** Frontal radiograph shows a widened and bifurcated anterior end of the left fifth rib (arrows).

portion of the rib and tend to manifest with more diaphyseal lesions rather than metaphyseal or epiphyseal lesions in long bones (5).

Nonaggressive Bone Lesions: Benign Tumors and Tumorlike Lesions

On radiographs, nonaggressive imaging features of rib lesions are similar to those found in the long bones. Lesions are usually geographic (a well-defined margin with or without sclerotic borders), with a narrow zone of transition and a smooth and uniform periosteal reaction without interruption (if present), and without an associated soft-tissue mass. Chondroid tumors (such as osteochondroma and enchondroma) and fibrous dysplasia are relatively frequent among nonaggressive rib lesions in children. Mesenchymal hamartoma and tuberous sclerosis complex (TSC), although rare, have distinctive imaging features.

Osteochondroma.—Osteochondroma is a cartilage-capped osseous excrescence and represents the most common benign tumor of the ribs (1). It is prevalent in children and adolescents, with approximately 80% of symptomatic cases diagnosed in patients aged 20 years or younger (6). Osteochondroma can occur in any bone that grows by endochondral ossification but is by far more common in the long bones of the extremities. In the ribs, it tends to occur at the costochondral junction (7).

An osteochondroma that projects outward may manifest as a palpable chest wall mass. An osteochondroma that projects inward is usually asymptomatic but may cause hemothorax, pneumothorax, or impingement on the intercostal neurovascular bundle (8). Most cases are monostotic. Polyostotic lesions are associated with multiple hereditary exostoses, which are caused by germ line mutations of the *EXT1* or *EXT2* gene and are associated with a higher risk for malignant transformation (chondrosarcoma). In multiple hereditary exostosis, up to 40% of the cases include rib involvement (6).

Diagnostic findings of solitary osteochondroma on chest radiographs include an exophytic bone projection with corticomedullary continuity to its original bone (Fig 4). However, some lesions may be mistaken for a pulmonary nodule if corticomedullary continuity is not apparent and also may simulate rib fractures. CT findings can confirm the diagnosis, especially for smaller lesions. MRI allows accurate assessment of the cartilage cap and potential malignant transformation.

Enchondroma.—Enchondroma is an intraosseous hyaline cartilage tumor and is relatively frequent among benign tumor of the ribs. Enchondromas in the ribs predominantly occur at the costochondral junction (1,9). Polyostotic lesions indicate an underlying condition such as Ollier disease or Maffucci syndrome (with soft-tissue hemangiomas) caused by somatic mutations of the *IDH1* or *IDH2* gene. The enchondromas associated with these syndromes are at higher risk of malignant transformation than is a solitary enchondroma.

On chest radiographs, an enchondroma appears as a geographic lucent intramedullary lesion with lobulated borders and endosteal scalloping (Fig 5). Intralesional chondroid matrix may show rings and arcs calcification, which is confirmatory when present. MRI can better depict intralesional cartilage matrices that are hyperintense on T2-weighted images.

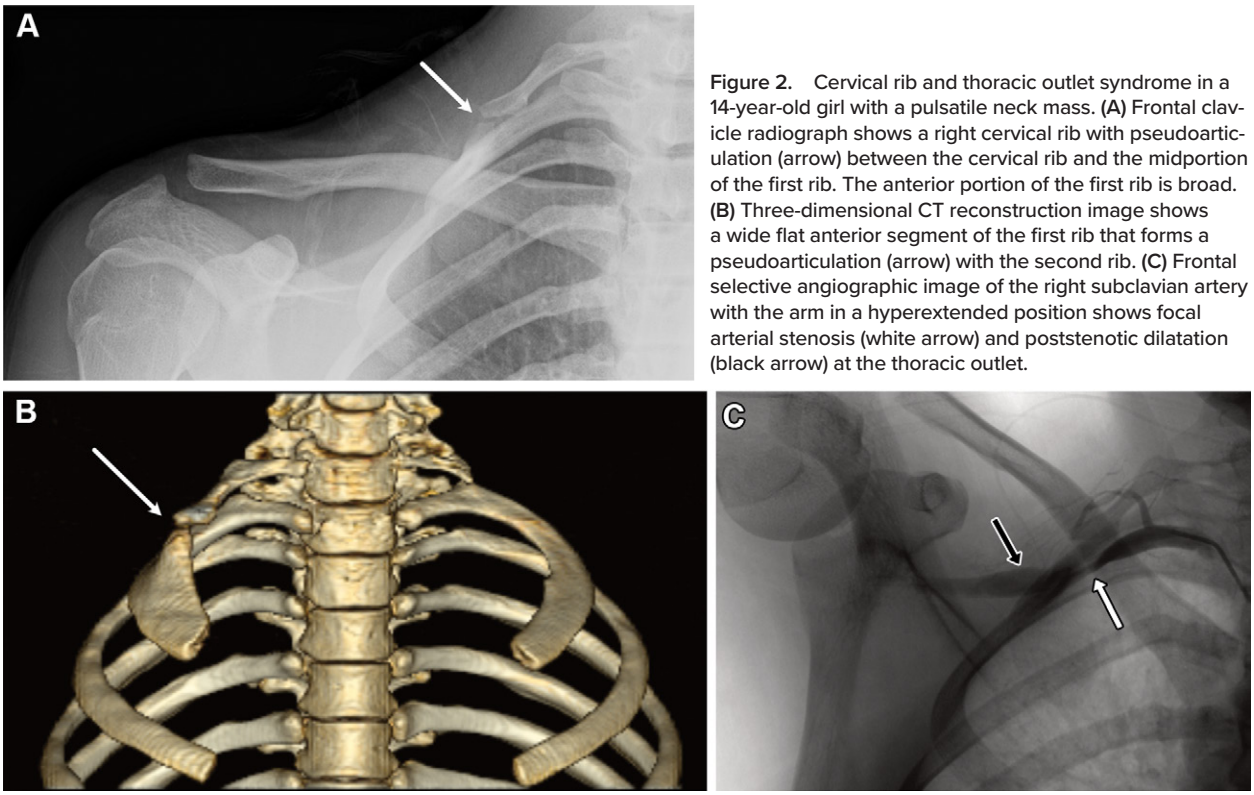

Figure 2. Cervical rib and thoracic outlet syndrome in a 14-year-old girl with a pulsatile neck mass. **(A)** Frontal clavicle radiograph shows a right cervical rib with pseudoarticulation (arrow) between the cervical rib and the midportion of the first rib. The anterior portion of the first rib is broad. **(B)** Three-dimensional CT reconstruction image shows a wide flat anterior segment of the first rib that forms a pseudoarticulation (arrow) with the second rib. **(C)** Frontal selective angiographic image of the right subclavian artery with the arm in a hyperextended position shows focal arterial stenosis (white arrow) and poststenotic dilatation (black arrow) at the thoracic outlet.

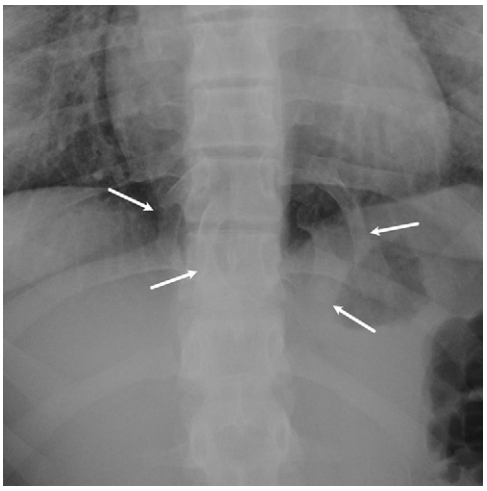

Figure 3. Intrathoracic ribs in a 16-year-old adolescent girl. Frontal radiograph shows bilateral supernumerary ribs (arrows) that arise from bilateral 10th costovertebral junctions and extend inferiorly.

Fibrous Dysplasia.—Fibrous dysplasia is an intramedullary fibro-osseous lesion caused by somatic activating mutations in the *GNAS* gene. It can occur at any age. Most cases are monostotic, and fibrous dysplasia has a predilection for the lateral and posterior aspect of the rib (1,9,10). More than half of polyostotic cases involve the ribs (often multiple ribs) and may cause thoracic wall deformity. Polyostotic fibrous dysplasia can be seen in patients with McCune-Albright syndrome (associated with café-au-lait spots and precocious puberty). On chest radiographs, fibrous dysplasia manifests as a geographic, fusiform, expansile lesion with heterogeneous internal architecture that may be radiolucent, be sclerotic, or have a ground-glass appearance depending on the proportion of fibrous and osseous components (Fig 6). MR images depict variable signal intensity on T2-weighted images depending on the internal components of the lesion.

Aneurysmal Bone Cyst.—Aneurysmal bone cyst (ABC), so named because of its expansile morphology and internal blood component, is a multiloculated cystic mass filled with blood products. It is more common in long bones and vertebrae and tends to be seen in adults but can be seen in the ribs in children (10,11). Initial symptoms may include pain, a palpable mass, and possibly a pathologic fracture, although often cases are identified incidentally at imaging (12).

ABC is classified into primary and secondary types. The primary type is isolated, whereas the secondary type is concomitant with a primary bone lesion such as giant cell tumor, fibrous dysplasia, and malignant tumors. On chest radiographs, ABC is depicted as a geographic expansile lucent bone lesion with internal thin septa (Fig 7). MR images depict multiple fluid-fluid levels, the finding of which is diagnostic for primary ABC in the absence of an associated soft-tissue mass.

Mesenchymal Hamartoma of the Chest Wall.—Mesenchymal hamartoma of the chest wall, which is a rare developmental anomaly rather than a true neoplasm, contains mature osteocartilaginous components (13,14). Like many lesions, mesenchymal hamartoma can also be seen in conjunction with ABC. This hamartomatous disorder is depicted as a large thoracic mass in neonates or infants and can even be diagnosed prenatally. Growth of the lesion spontaneously ceases by 1 year of age. On chest radiographs, mesenchymal

Table 2: Focal Rib Abnormalities

Entity	Imaging Findings	Notes
Nonaggressive bone lesions (benign tumors and tumorlike lesions)		
Osteochondroma	Exophytic bone projection with corticomedullary continuity	Associated with hereditary multiple exostoses
Enchondroma	Localized lucent lesion with lobulated border and rings and arcs calcification	Associated with Ollier and Maffucci syndromes
Fibrous dysplasia	Fusiform lesion with various internal attenuation but typically a ground-glass appearance	Associated with McCune-Albright syndrome
ABC	Expansile lesion with internal thin septa; fluid-fluid levels on MR images	...
Mesenchymal hamartoma	Large mass with comblike osseous projection eroding adjacent ribs	Congenital hamartoma, often associated with ABC
Tuberous sclerosis complex	Tiny osteosclerotic foci; only detected on CT and MR images	...
Aggressive bone lesions (malignant tumors)		
Ewing sarcoma family of tumors	Aggressive bone destruction with large extraosseous component	Chromosomal translocations t (11;22)(q24;q12) in tumor cells
Osteosarcoma	Aggressive bone destruction with extraosseous component containing osseous matrices	Osteoid matrix more clearly delineated on CT images
Neuroblastoma	Destructive lesion of the posterior ribs	Positive at metaiodobenzylguanidine imaging
Lymphoma	Destructive lesion	Restricted diffusion on MR images and FDG avidity on PET/CT images
LCH	Intermediate bone destruction but may appear as if aggressive	Difficult to distinguish from inflammatory conditions
Intermediate bone lesions (infectious and inflammatory disorders)		
Osteomyelitis	Variable manifestations depending on the stage	Abscess shows reduced diffusivity on diffusion-weighted images
Infantile cortical hyperostosis	Periosteal new bone formation and later diaphyseal expansion	A self-limiting disease in infancy, abnormal type 1 collagen (a specific mutation in *COL1A1*) in some patients
Prostaglandin-induced cortical hyperostosis	Periosteal new bone formation, symmetric and widespread	Indistinguishable from Caffey disease on radiologic grounds
CNO	Variable manifestations depending on the stage	A self-limiting disease in infancy, a specific mutation in *COL1A1* in a subgroup

Note.—ABC = aneurysmal bone cyst, CNO = chronic nonbacterial osteomyelitis, FDG = fluorodeoxyglucose, LCH = Langerhans cell histiocytosis.

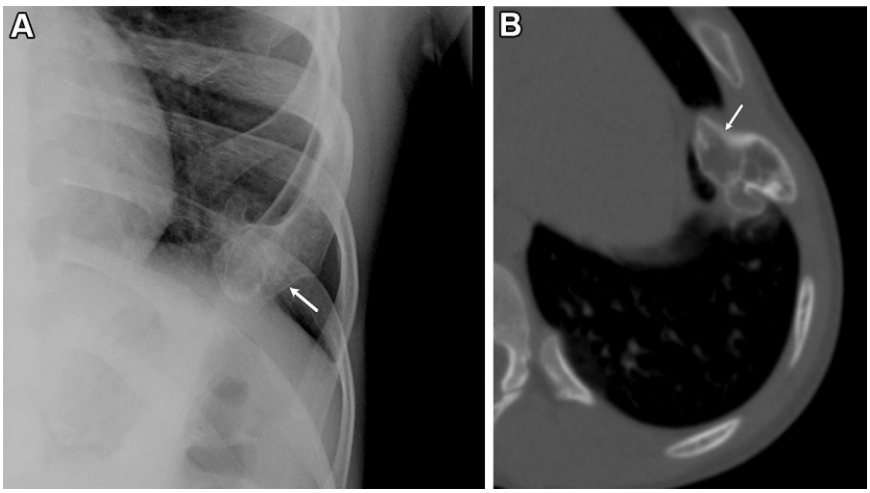

Figure 4. Osteochondroma in a 14-year-old boy with multiple hereditary exostoses. **(A)** Frontal chest radiograph shows an osseous ingrowth (arrow) at the anterior aspect of the left seventh rib. **(B)** Axial CT image of the chest shows an osseous protuberance with corticomedullary continuity (arrow).

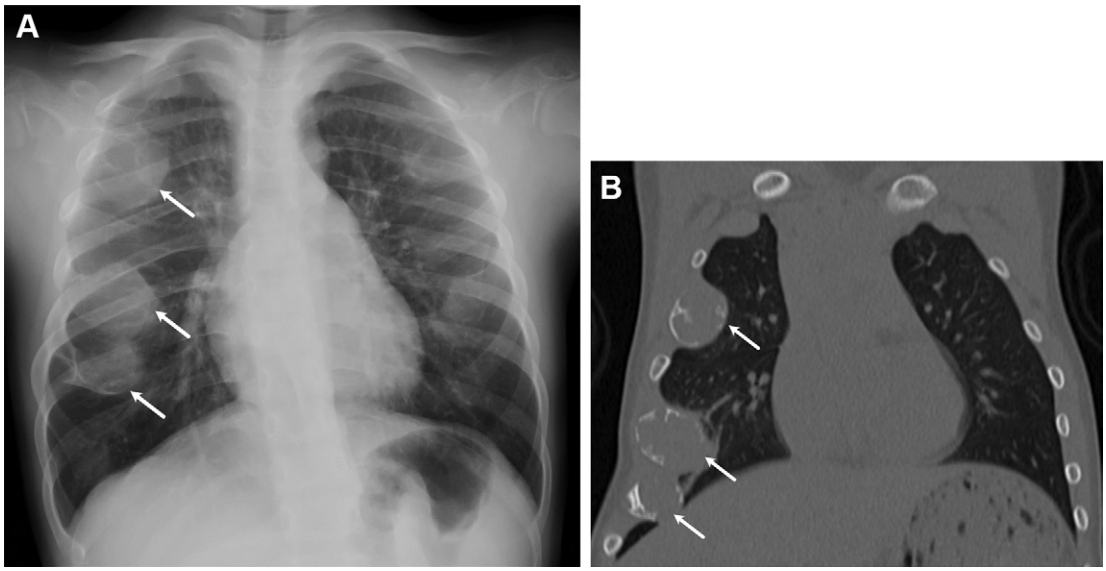

Figure 5. Multiple enchondromas (Ollier disease) in a 4-year-old girl. **(A)** Frontal chest radiograph shows multiple well-defined expansile lucent lesions at the costochondral junction with the largest lesions at the right third, fifth, and sixth ribs (arrows). **(B)** Coronal CT image of the chest shows multilobulated expansile intraosseous lesions with endosteal scalloping and cortical thinning (arrows) consistent with enchondromas. There is no soft-tissue mass or periosteal reaction.

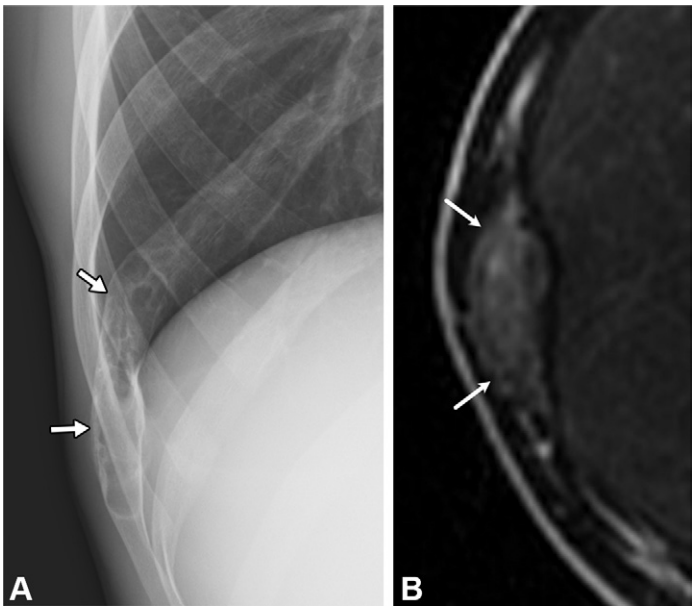

Figure 6. Fibrous dysplasia in a 16-year-old adolescent boy. **(A)** Frontal chest radiograph shows an elongated lucent lesion (arrows) intervened by ground-glass opacities in the posterolateral aspect of the right ninth rib. **(B)** Axial T2-weighted MR image shows a well-defined lesion (arrows) with heterogeneous signal intensity composed of intermediate signal intensity mixed with areas of hypointensity and smaller areas of hyperintensity.

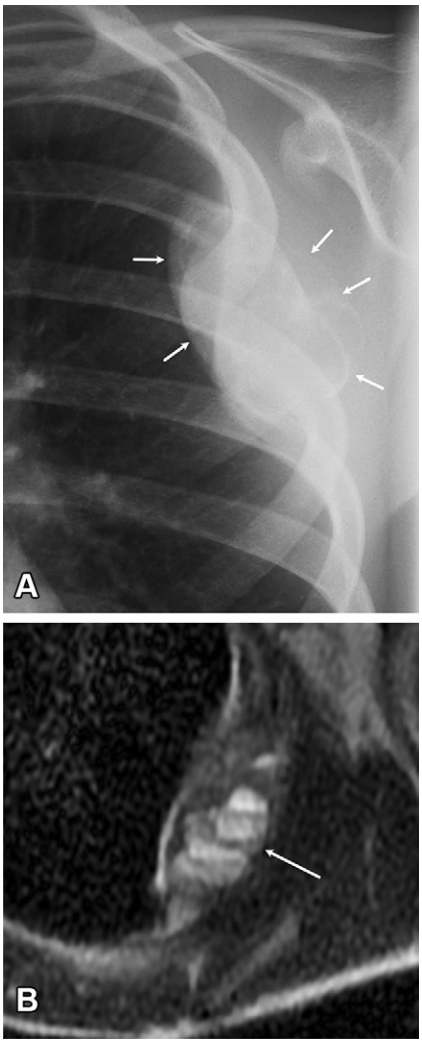

Figure 7. ABC in a 9-year-old boy. **(A)** Frontal chest radiograph shows a large expansile osteolytic lesion with a sharply defined multilobulated border (arrows) involving the left fourth rib. The outer cortex is extremely thinned. **(B)** Axial T2-weighted image shows multilocular cystic lesions (arrow) with internal fluid-fluid levels without solid components.

hamartoma manifests as a large extrapleural mass associated with erosions in one or more adjacent ribs and calcification and/or ossification that may be described as comblike or spurlike osseous projections (Fig 8). CT and MRI better delineate these distinctive findings (13,14).

Tuberous Sclerosis Complex.—TSC is an autosomal dominant genetic disorder characterized by hamartomatous lesions in multiple organs caused by mutations in *TSC1* or *TSC2* genes (tumor suppressor genes). Patients with TSC may present with sclerotic lesions of the posterior ribs, vertebral bodies, and iliac side of the sacroiliac joints that measure only a few millimeters in size (15). It is speculated that mutations of these genes cause hyperactivation of the mammalian target of rapamycin pathway, which then leads to overexpression of osteoblasts. Small sclerotic foci on CT images are quite common in TSC and detected in approximately 90% of affected individuals

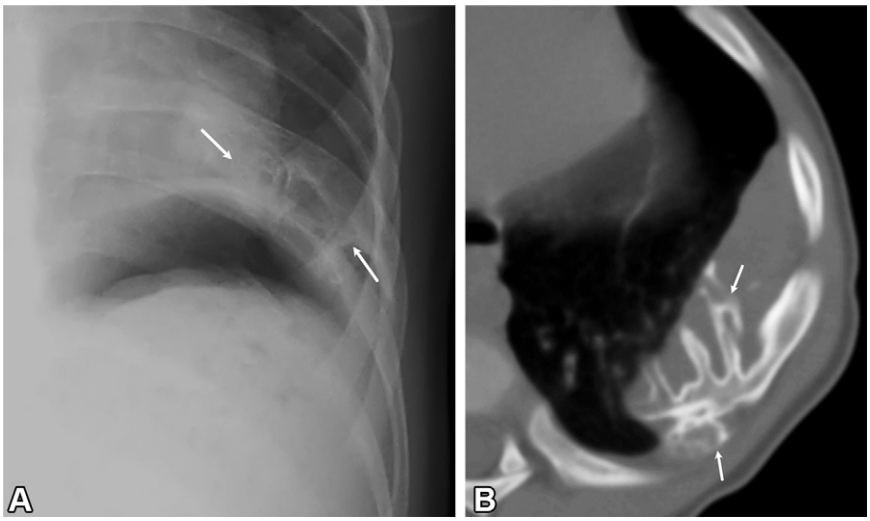

Figure 8. Mesenchymal hamartoma of the chest wall in a 1-year-old boy. **(A)** Frontal chest radiograph shows broadening and an irregular contour of the posterolateral left eighth rib associated with a large soft-tissue area of attenuation. Spurlike bone projections (arrows) arise from the inferior aspect of the eighth rib. **(B)** Axial CT image of the chest shows a large extrapleural mass associated with comblike bone projections stemming from the broad irregular eighth rib (arrows).

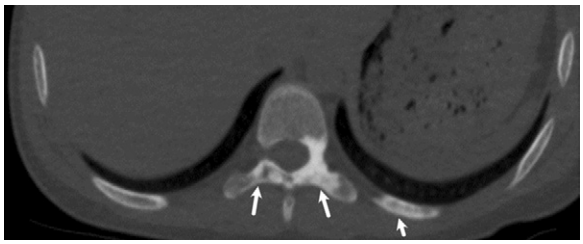

Figure 9. Sclerotic changes in a rib and the spine in a 16-year-old adolescent girl with TSC. Axial CT image of the chest shows multiple sclerotic lesions involving the left ninth rib and posterior arches of the ninth thoracic vertebra (arrows).

(16,17). This finding is not specific but highly suggestive of TSC (Fig 9). Although rare, fibrous dysplasialike sclerotic lesions with osseous enlargement and deformity leading to a thoracic deformity have also been reported (18).

Aggressive Bone Lesions: Malignant Tumors

Aggressive features of rib lesions on chest radiographs include ill-defined margins with a wide zone of transition, permeative or "moth-eaten" areas of bone destruction, an irregular periosteal reaction, and an associated soft-tissue mass. The Ewing sarcoma family of tumors is the most common primary malignant tumor that occurs in the ribs. Osteosarcoma, the most common malignant bone tumor overall in the pediatric age group, may rarely involve the ribs. Neuroblastoma arising from the posterior mediastinum may locally invade adjacent ribs. Neuroblastoma is also the most common metastatic tumor involving the ribs. Lymphoma and leukemia may manifest with aggressive rib lesions. Langerhans cell histiocytosis (LCH) is a malignancy-like condition that is also discussed given that it often manifests with aggressive features indistinguishable from those of malignancy.

Ewing Sarcoma Family of Tumors.—Ewing sarcoma family of tumors comprise a group of malignancies (Ewing sarcoma, peripheral primitive neuroectodermal tumors, and Askin tumor) that encompass the most common primary chest wall malignancy in the pediatric age group. Histologically, these tumors are composed of small round cells with homogeneous immunohistochemical and molecular properties. Chromosomal translocations t(11;22)(q24;q12) are seen in 80%–95% of cases. The peak age of onset is 10–15 years (19).

This sarcoma family typically manifests as a rapidly growing painful chest wall mass. Chest radiograph findings include permeative bone destruction and aggressive periosteal reaction. When detected early, it manifests primarily as a bone lesion. However, it often remains undetected until the disease has advanced, at which point it can be associated with an extraosseous mass that can be larger than the intraosseous lesion (Fig 10) (4,7). Sclerotic changes can be seen in less than 20% of cases (5). MR images show heterogeneous signal intensity and variable enhancement after intravenous contrast material administration, reflecting the presence of both solid and necrotic components. Pleural invasion results in a large amount of pleural fluid that may be present at initial presentation (7,19). CT or MRI is necessary to evaluate the extent of the tumor and associated intrathoracic abnormalities.

Osteosarcoma.—Primary osteosarcoma of the rib is rare and accounts for only 1%–2% of all cases of osteosarcoma (7,20). Age prevalence is the same as that for osteosarcoma in other sites, with an average age at diagnosis of 13 years (21). The lungs are the most common site of metastasis. The prognosis is usually good if metastases are not present at the time of diagnosis (21).

Chest radiograph features include aggressive areas of bone destruction and large extraosseous components containing osteoid matrices (Fig 11). CT is useful to help ascertain the presence of unique osteoid matrices (ie, dense and cloudy foci of high attenuation that tend to be centrally located) (20,22). MRI findings include hypointensity on T1-weighted images, heterogeneous signal intensity on T2-weighted images, and heterogeneous enhancement after contrast material administration, reflecting the heterogeneity of its internal components with possible areas of necrosis (22,23).

Neuroblastoma.—Neuroblastoma is a neoplasm arising from the neural crest and represents the most common extracranial malignant tumor in children (24). Neuroblastoma most

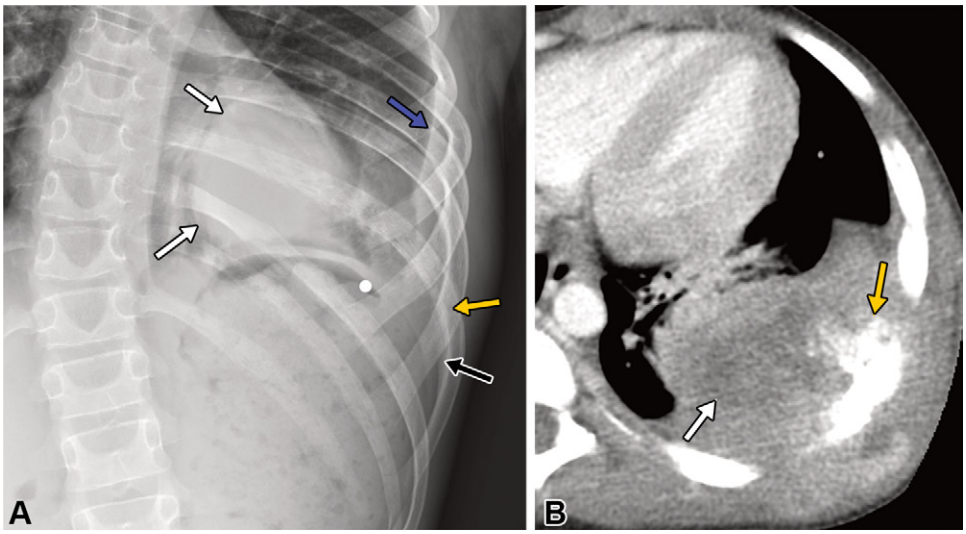

Figure 10. Ewing sarcoma family of tumor in a 10-year-old boy. **(A)** Frontal chest radiograph shows a large retrocardiac soft-tissue mass (white arrows) associated with permeative destruction (yellow arrow) and irregular periosteal reaction (black arrow) of the ninth rib as well as intercostal space widening. A small amount of pleural effusion (blue arrow) is also depicted. The spine shows a right convex curvature. **(B)** Axial contrast-enhanced CT image of the chest shows a large soft-tissue mass extending into the thoracic cavity and the chest wall with internal necrosis (white arrow) and eighth rib destruction with sunburstlike periosteal reaction (yellow arrow).

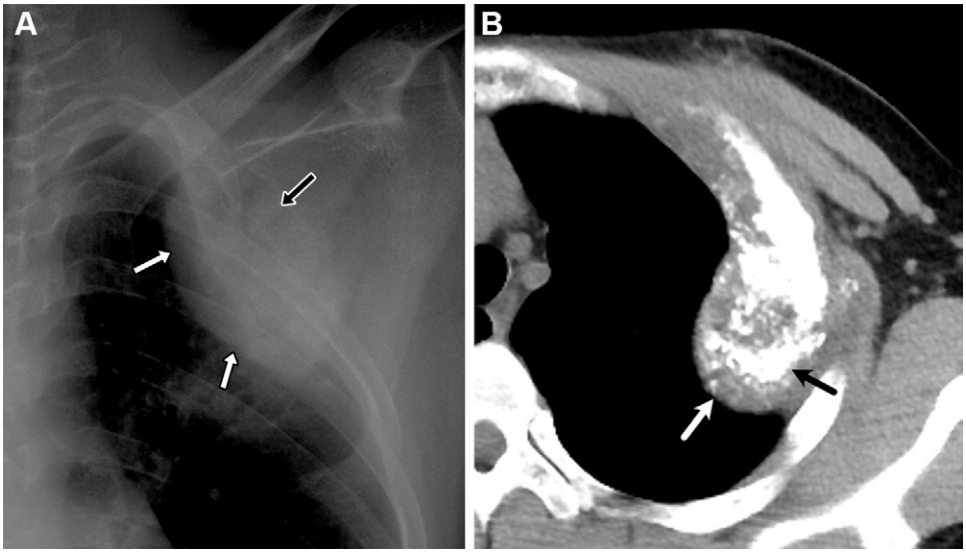

Figure 11. Osteosarcoma in a 17-year-old adolescent boy. **(A)** Frontal chest radiograph shows a large destructive lesion of the second rib with loss of cortical margins (white arrows) and dense cloudy internal attenuation (black arrow). **(B)** Axial CT image of the chest shows aggressive bone destruction (white arrow) with an extensive osteoid matrix (black arrow).

commonly affects children under 5 years of age. Thoracic neuroblastoma typically arises in the posterior mediastinum and is estimated to comprise 11%–26% of all neuroblastomas. Due to its proximity, posterior mediastinal neuroblastoma often invades the ribs (25).

Chest radiographs depict a rapidly progressive destructive osseous lesion associated with a posterior mediastinal mass (Fig 12). CT and MR images depict an aggressive-appearing mass with heterogeneous internal attenuation and signal intensity due to hemorrhage and necrosis. Intraspinal extension of the posterior mediastinal mass is not uncommon. In addition, neuroblastoma is the most common metastatic tumor of the chest wall in children. These metastatic lesions may show lytic lesions with a wide zone of transition associated with periosteal reaction.

Nuclear scintigraphy studies such as metaiodobenzylguanidine imaging or technetium 99m–labeled methylene diphosphonate bone scintigraphy are more sensitive for the detection of small metastatic lesions. Notably, a new dynamic gallium-68 tetraazacyclododecane tetraacetic acid–octreotate (DOTATATE) PET/CT radiotracer has been introduced that has better lesion conspicuity, higher sensitivity and specificity, and improved spatial resolution (26). Although currently off-label in the pediatric population, the use of DOTATATE in children is being explored.

Lymphoma.—Primary bone lymphoma accounts for less than 5% of primary bone malignancies in childhood and predominantly involves the long bones. Primary rib involvement is very rare. Most primary bone lymphomas are non-Hodgkin lymphomas, among which diffuse large B-cell lymphoma is the most common (7,27). Primary bone lymphoma can occur at any age, with reported cases in children as young as 2 years old and teenaged patients, although it is relatively rare in this age group (28). Chest radiographs depict a permeative lytic lesion often accompanied by periosteal reaction (Fig 13). MRI demonstrates a localized bone marrow–replacing lesion with periosteal reaction and a soft-tissue mass without cortical destruction (28). Diffusion-weighted images depict restricted diffusion reflecting high cellularity. Fluorodeoxyglucose (FDG) PET images depict avid uptake that can be useful for initial staging and evaluating treatment response.

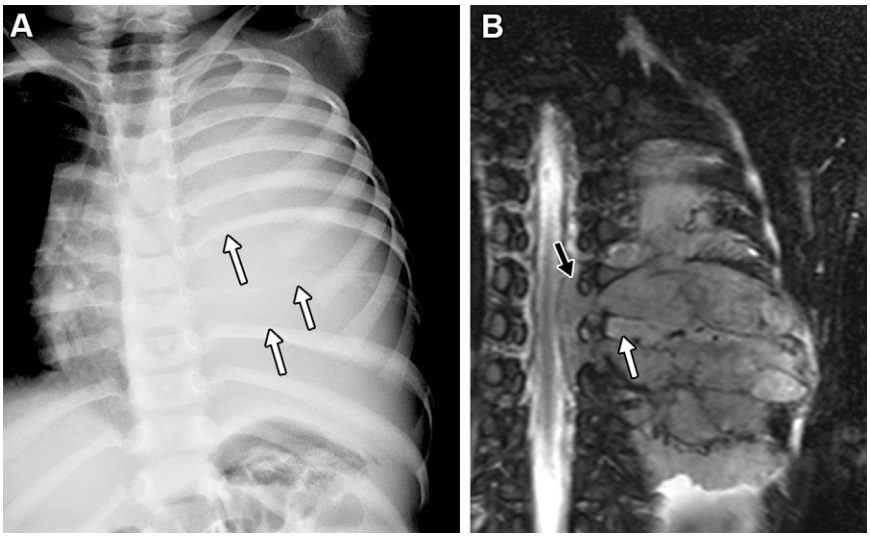

Figure 12. Neuroblastoma of the posterior mediastinum with rib involvement in a 3-year-old boy. **(A)** Frontal chest radiograph shows a complete opacification of the left hemithorax with a tracheal deviation to the right. The posterior segment of the left seventh, eighth, and ninth ribs is eroded (white arrows) with permeative destruction extending into the lateral segment of the eighth rib. **(B)** Coronal fat-suppressed T2-weighted MR image shows an extensive posterior mediastinal mass spreading through the extrapleural space, extending into the spinal canal (black arrow) and invading the eighth rib (white arrow).

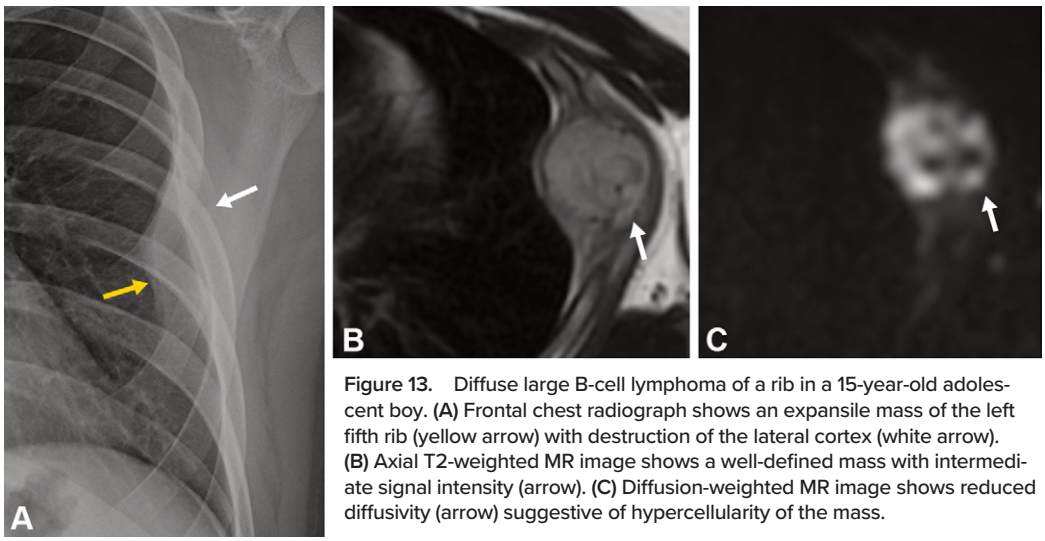

Figure 13. Diffuse large B-cell lymphoma of a rib in a 15-year-old adolescent boy. **(A)** Frontal chest radiograph shows an expansile mass of the left fifth rib (yellow arrow) with destruction of the lateral cortex (white arrow). **(B)** Axial T2-weighted MR image shows a well-defined mass with intermediate signal intensity (arrow). **(C)** Diffusion-weighted MR image shows reduced diffusivity (arrow) suggestive of hypercellularity of the mass.

Langerhans Cell Histiocytosis.—LCH is a condition characterized by proliferation of abnormal dendritic histiocytes, with a peak age of onset between 1 and 4 years (29). LCH can be localized to a single organ or disseminated to multiple organs. About 80% of the cases are associated with bone changes, predominantly involving flat bones such as the skull, vertebrae, pelvis, mandible, and ribs (30,31).

Imaging findings vary depending on the disease stage. In the early stage, LCH manifests as an aggressive process simulating malignancy with the imaging findings of a destructive osteolytic lesion associated with interrupted periosteal reactions and extraosseous edematous changes and a soft-tissue mass (Fig 14). In the late stage, LCH demonstrates more nonaggressive imaging features such as a localized osteolytic lesion with reactive sclerosis (32). Vertebra plana (collapsed vertebral body, a finding characteristic of LCH) may also be depicted on chest radiographs, especially on the lateral view. Whole-body imaging such as bone scintigraphy, whole-body MRI, and FDG PET is useful to delineate additional sites of disease. Often, LCH lesions require biopsy to exclude infection or malignancy.

Infectious and Inflammatory Disorders

Infectious or inflammatory disorders of the ribs are common and include osteomyelitis, infantile cortical hyperostosis, and chronic nonbacterial osteomyelitis (CNO, alternatively called chronic recurrent multifocal osteomyelitis). The imaging findings of these disorders overlap with those of aggressive bone tumors. Although the findings at clinical presentation usually allow differentiation, biopsy may be warranted to confirm the diagnosis.

Osteomyelitis.—Pyogenic osteomyelitis of the rib is uncommon, accounting for less than 1% of all pediatric osteomyelitis (33). Direct spread of intrathoracic infection (eg, empyema) into the adjacent rib can occur. Hematogenous spread to the rib tends to occur at the costochondral junction (metaphyseal equivalent) (34). In most cases, affected children show clinical signs of infection such as fever and pain. However, these symptoms may not be apparent with indolent pathogens (eg, *Salmonella*, *Mycobacterium tuberculosis*, fungi, and bacillus Calmette-Guérin vaccination).

Chest radiograph findings of rib osteomyelitis recapitulate those of the tubular bones, such as focal lytic change, bone

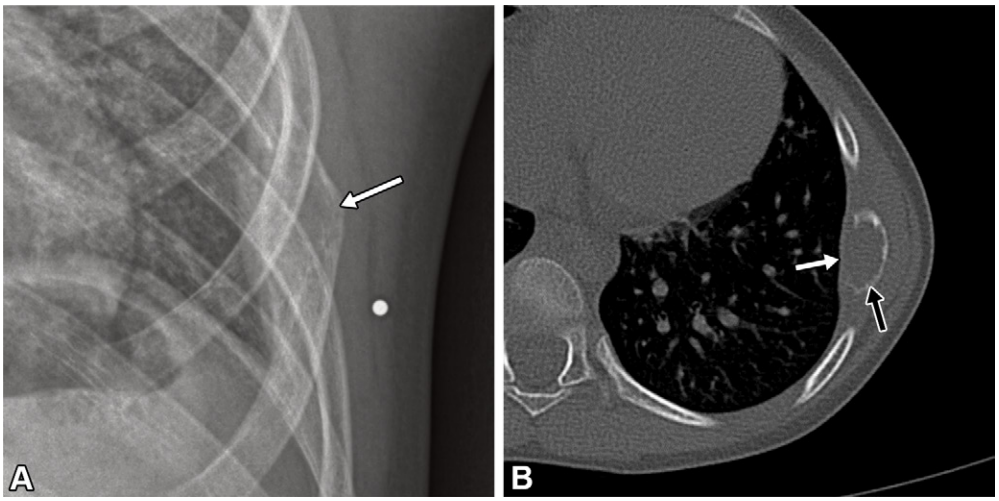

Figure 14. LCH of a rib in a 5-year-old boy who presented with chest pain. **(A)** Frontal chest radiograph shows a slightly aggressive expansile osseous lesion of the lateral segment of the left seventh rib (white arrow). **(B)** Axial CT image of the chest shows a focal expansile osteolytic lesion (black arrow) with a moth-eaten type of cortical destruction (white arrow) without an extraosseous soft-tissue mass or internal matrix.

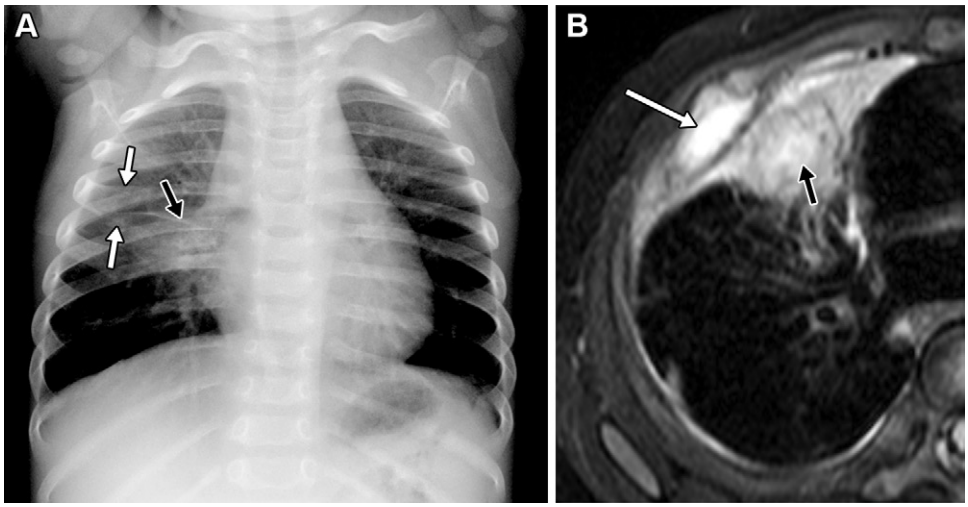

Figure 15. Osteomyelitis of a rib associated with pneumonia in a 7-month-old girl. **(A)** Frontal chest radiograph shows expansion of the anterior end of the right fourth rib (white arrows) with adjacent airspace opacification and thickening of the interlobar fissure (black arrow). **(B)** Axial postcontrast fat-suppressed T1-weighted MR image shows abnormal bone marrow enhancement (white arrow) associated with lung consolidation (black arrow).

destruction, periosteal reaction, and reparative sclerosis (Fig 15). However, these changes are absent in the acute phase. MRI is more sensitive for detection of early bone marrow signal intensity changes, which include geographic marrow-replacing lesions with hypointensity on T1-weighted images and heterogeneous hyperintensity on T2-weighted images associated with contrast enhancement. CT is inferior to MRI for the diagnosis of acute osteomyelitis (34), although CT may be useful for evaluating concomitant intrathoracic pathologic features.

Infantile Cortical Hyperostosis.—Infantile cortical hyperostosis (Caffey disease) is a sterile inflammatory periostitis that occurs in infancy (6 weeks to 6 months of age) and is clinically characterized by fever, irritability, and soft-tissue swelling. The etiology has not been determined, and the disease is self-limited (35). A subset of patients with this disorder share a disease-specific mutation in type 1 collagen gene (*COL1A1*) (35). Most cases are polyostotic with a predilection for the mandible (seen in 70%–90% of cases), clavicles, scapulae, and ribs (36).

Chest radiograph findings depend on disease stage, ranging from periosteal new bone formation in early stages to diaphyseal expansion and bone remodeling in more mature stages (Fig 16). Osseous bridging between adjacent ribs may occur that may later lead to scoliosis. MRI has higher sensitivity for detection of early periostitis, intraosseous edema, and juxtaosseous soft-tissue edema (37).

Prostaglandin-induced Cortical Hyperostosis.—Prostaglandin (E-type) is often administered to neonates with cyanotic heart disease to maintain the patency of the ductus arteriosus in ductal-dependent congenital heart disease. This treatment is typically used for a short period until the neonate can undergo cardiac surgery. However, prolonged use of prostaglandin E, as seen in preterm neonates, can lead to cortical hyperostosis or periosteal new bone formation in a dose- and duration-dependent manner (38). While the long bones of the extremities are the most commonly affected, the ribs, scapula, and clavicles may also be involved (39). This condition is usually asymptomatic and self-limited. Diagnosis is straightforward based on the patient's medication history. (38) (39).

Chronic Nonbacterial Osteomyelitis.—CNO is an autoinflammatory disorder of unknown etiology (40) characterized by aseptic bone inflammation that may follow a relapsing and

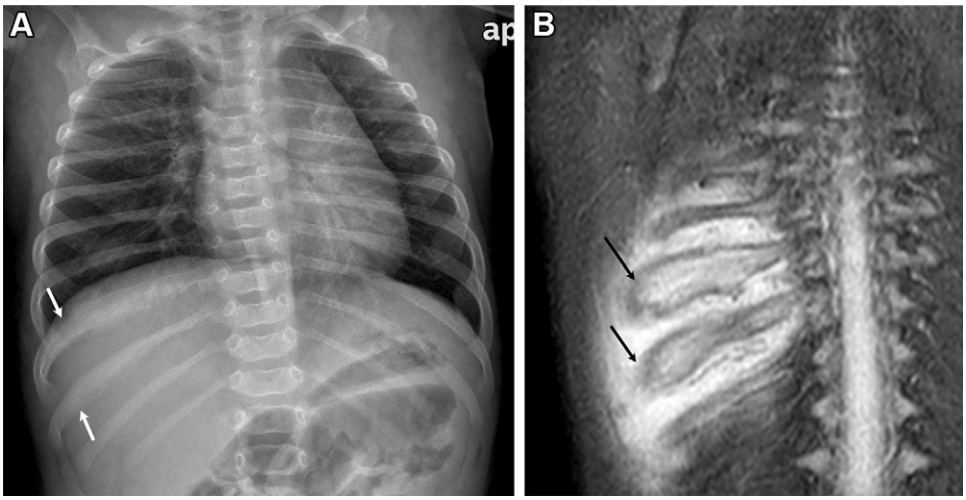

Figure 16. Caffey disease in a 3-month-old boy. **(A)** Frontal chest radiograph shows cortical hyperostosis of the right ninth and tenth ribs (arrows). **(B)** Coronal fat-suppressed T2-weighted MR image shows cortical expansion and bone marrow edema of the ribs associated with adjacent intercostal soft-tissue edema (arrows). (Figure courtesy of Talaat Youssef, PhD, FRCR, FFRCSI, Sidea Medicine, Doha, Qatar.)

Table 3: Multifocal Rib Abnormalities

Entity	Imaging Findings	Notes
Rib notching and/or twisted ribs		
Coarctation of the aorta	Inferior edge erosion from the third to the eighth ribs	Also seen in systemic arterial collaterals and intercostal arteriovenous malformation
NF1	Inferior edge erosion due to neurofibromas or distortion due to mesodermal dysplasia	Mesodermal dysplasia may cause distortion of other bones
Vanishing ribs		
Gorham-Stout disease	Rapidly progressive osteolysis and later disappearance of the ribs	May be associated with chylous thorax
Multifocal rib fractures with normal bone in shape		
Nonaccidental injury	Multiple fractures of different stages	Predilection to sites related to shaking
Rosary of the costochondral junction		
Rare manifestation of nonaccidental injury	Distorted costochondral junction	Reminiscent of metaphyseal corner fractures
Scurvy	Bulging of the costochondral junction	Scorbutic rosary due to repetitive injury to fragile bone
Rickets	Bulging of the costochondral junction	Rachitic rosary due to excessive undermineralized matrix

Note.—NF1 = neurofibromatosis type 1.

remitting course (41). The incidence is estimated at one in 1 million people (42). CNO lesions are commonly seen in the metaphyses and metaphyseal equivalents of long bones, mandible, clavicles, ribs, and pelvis (43). The average age of onset is 9–14 years old, and female patients are impacted twice as often as male patients (43–45).

Chest radiograph findings depend on disease stage and may be initially absent in the early stages. Localized osteolytic changes associated with sclerosis and periosteal reaction, followed by remodeling and resolution, are present in more mature stages of the disease. MRI is more sensitive for assisting in the detection of disease, particularly in the acute phase, depicting bone marrow edema signal intensity, periosteal reaction, and juxtaosseous soft-tissue edema. Intraosseous or periosteal abscess is absent. Whole-body MRI best demonstrates multifocal lesions that can help confirm diagnosis (43). For definitive diagnosis, a biopsy is often required to exclude pyogenic osteomyelitis or neoplasm.

Multifocal Rib Abnormalities

Rib notching, rib twisting, vanishing ribs, and multiple or multifocal rib fractures are types of nonneoplastic and noninfectious rib anomalies that may be incidentally encountered at imaging and warrant dedicated discussion (Table 3).

Rib Notching and Rib Twisting

Rib notching is a sequela of chronic pressure erosion caused by enlarged intercostal arteries that course along the inferior surface of the ribs. Rib notching has been historically considered a classic radiologic finding of aortic coarctation (Fig 17). However, rib notching due to aortic coarctation is rarely seen today due to the earlier detection and treatment of aortic coarctation that prevents the collateral arteries (which contribute to the notched appearance) from having a chance to develop (4).

Rib notching may also be caused by collateral arterial pathways in severe pulmonary artery stenosis and intercostal

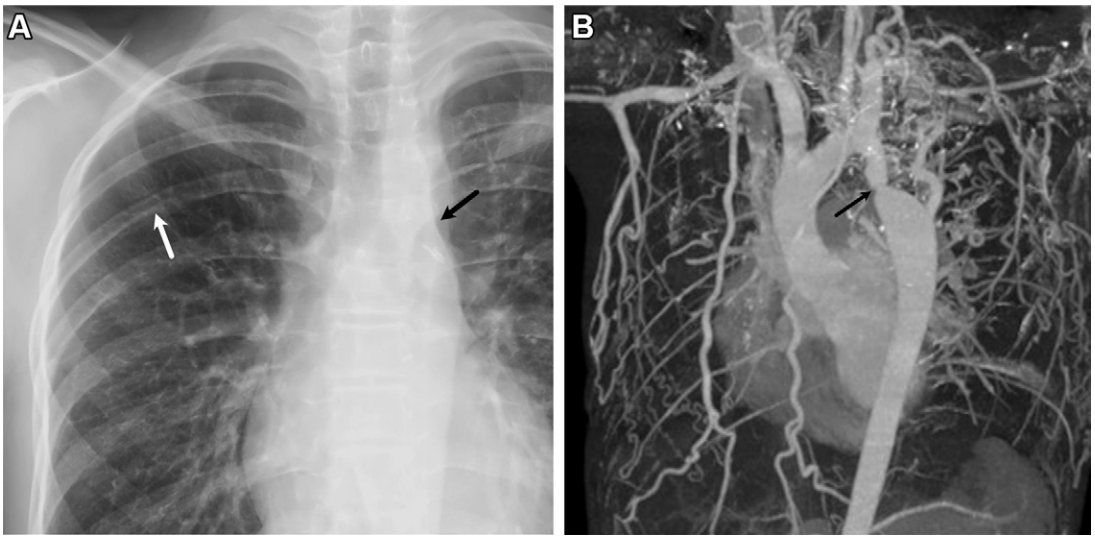

Figure 17. Rib notching in a 10-year-old-boy with untreated aortic coarctation. **(A)** Frontal chest radiograph shows mild thinning with sclerosis of the inferior margin of the bilateral third to fifth posterior ribs. Focal notching is evident in the inferior margin of the right fifth rib (white arrow). The aorta shows indentation of the aortic contour (black arrow; "figure 3" sign). **(B)** Three-dimensional reconstruction of a coronal contrast-enhanced chest CT image shows aortic coarctation (arrow) with prominent collateral pathways including intercostal arteries.

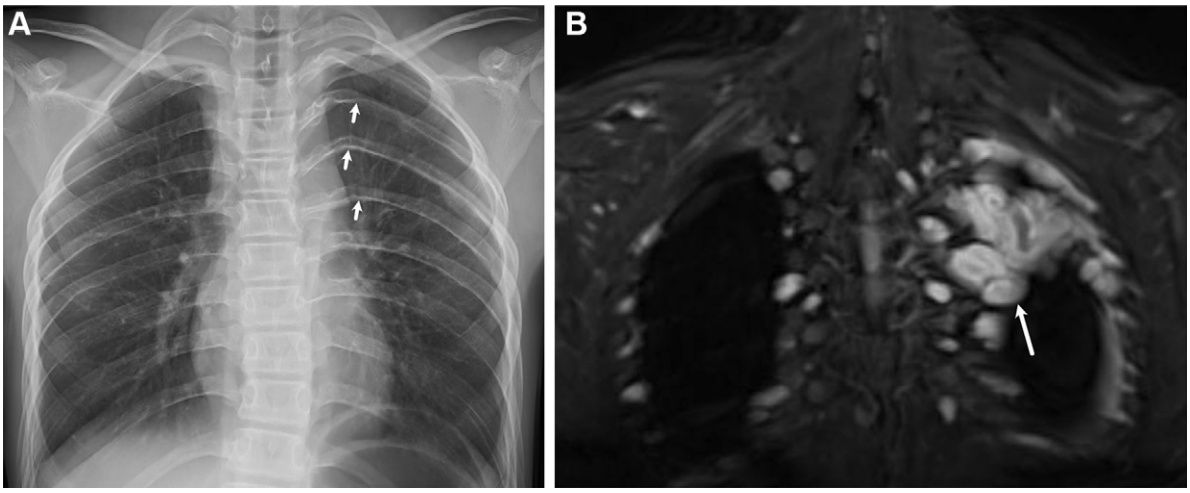

Figure 18. Rib notching and twisting in a 13-year-old girl with NF1. **(A)** Frontal chest radiograph shows rib notching and twisted rib deformity in bilateral upper ribs, which is much worse on the left (arrows). The left fourth rib shows severe rib notching with a ribbonlike appearance. **(B)** Coronal fat-suppressed T2-weighted MR image shows plexiform neurofibromas (arrow) extending along the intercostal nerves.

arteriovenous malformation. Rib notching can also be seen with neurofibromatosis type 1 (NF1) due to erosion by neurofibromas (Fig 18) or primary mesodermal dysplasia without adjacent focal neurofibroma (46). In the most severe form of rib notching in NF1, the individual rib may appear twisted ("ribbon rib"). Diffuse rib twisting involving multiple ribs is discussed later in the article.

Vanishing Ribs

Gorham-Stout disease (phantom or vanishing bone disease) is a disorder characterized by progressive osteolysis due to abnormal proliferation of lymphatic vessels (47,48). The ribs are commonly affected. It is a slowly progressive disease, and the patient usually remains asymptomatic. Polyostotic involvement is the rule. The initial disease manifestation on chest radiographs include focal osseous resorption of the ribs that worsens over time and eventually culminates in apparent disappearance of affected ribs, thus the name *vanishing bone disease* (Fig 19). Other commonly affected bones include the skull, clavicles, and cervical vertebrae. Extraskeletal involvement occurs in the lungs, mediastinum, abdominal cavity, and spleen (49).

Multifocal Rib Fractures

Nonaccidental injury should be suspected in children with multifocal rib fractures, particularly those under 2 years of age. Rib fractures may be identified at a skeletal survey when abuse is clinically suspected. However, they can also be incidentally depicted on routine chest radiographs (50,51). Rib fractures most often occur in the costal head, costotransverse junction, and posterior and lateral arcs depending on the mechanism of injury, which usually involves anteroposterior compression of the thorax during shaking. The fractures may be seen in variable stages of healing (Fig 20). Acute rib fractures may be difficult to detect on routine chest radiographs, and additional oblique views are helpful for this reason. The presence of callus formation on follow-up radiographs is also helpful to confirm the presence of fractures that are not visible at initial imaging.

The frequency of rib fractures on chest radiographs in confirmed cases of nonaccidental injury is reported to be up to 25%, while the incidence is 35% at postmortem evaluation, suggesting that a significant number of rib fractures are undiagnosed or undetectable on radiographs (52,53). Low-dose CT has the potential to increase the sensitivity for detection of rib fractures.

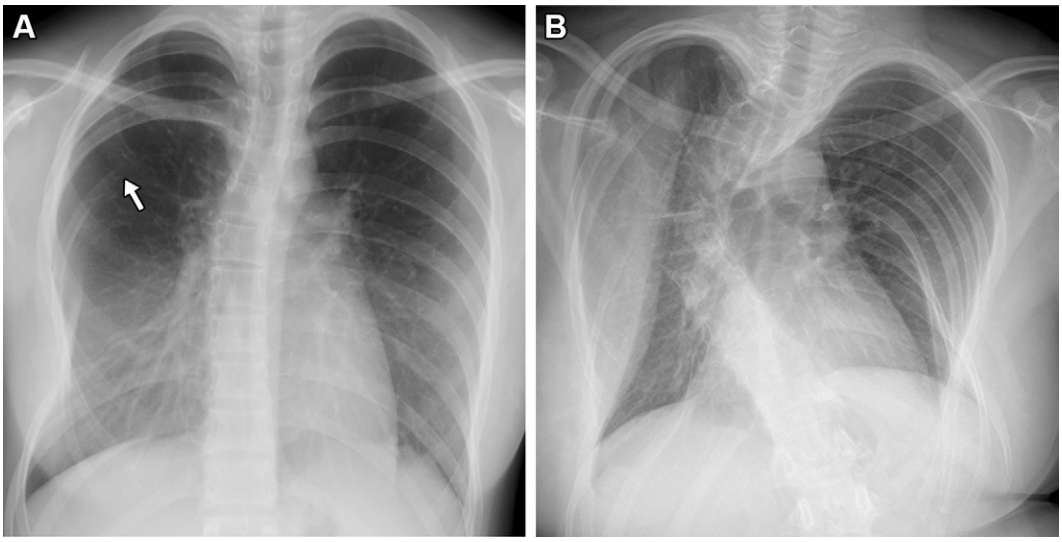

Figure 19. Vanishing ribs in a female patient with Gorham-Stout disease. **(A)** Frontal chest radiograph at 11 years of age shows thinning and resorption of the posterior right sixth (arrow) to ninth ribs with mild thoracic deformity and scoliosis. **(B)** Frontal chest radiograph at 21 years of age shows marked progression of rib vanishing, thoracic deformity, and scoliosis.

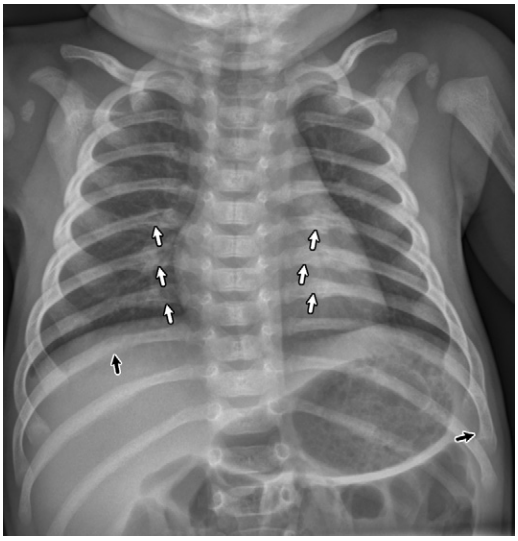

Figure 20. Nonaccidental trauma in a 1-month-old boy. Frontal chest radiograph shows multiple fractures of variable ages, including acute fractures (black arrows) of the left anterior ninth rib and right posterior ninth rib, as well as healing fractures of the bilateral sixth to eighth posterior ribs (white arrows).

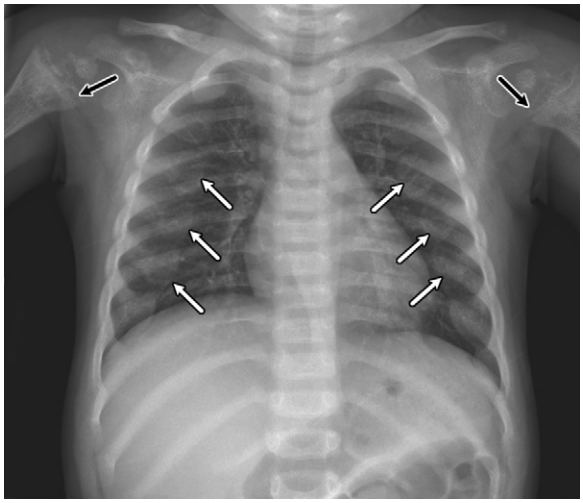

Figure 21. Rachitic rosary in a 1-year-old boy with vitamin D deficiency. Frontal chest radiograph shows bulbous enlargement of the costochondral junction (white arrows) and rachitic changes of the proximal humerus (black arrows) due to excessively undermineralized osteocartilaginous matrix.

Multifocal rib fractures are also a common finding in malnourished children, non–weight-bearing children (eg, intensive care unit patients), or individuals with congenital or acquired diseases that lead to poor ossification, such as osteogenesis imperfecta and rickets.

Rosary of the Costochondral Junction

Repetitive forces on the anterior thorax in patients with brittle ribs may cause chronic injury and reparative swelling of the costochondral junction. A classic example is scorbutic rosary seen in scurvy (vitamin C deficiency). Vitamin C deficiency impairs collagen production and subsequently causes vascular and skeletal fragility. This results in hemorrhagic diathesis and generalized osteoporosis accompanied by classic findings of scurvy of the long bones (ie, Wimberger ring sign, Frankel line, Trümmerfeld zone, and Pelkan spur or fracture). As with Pelkan fracture, injured costochondral junctions become prominent and are associated with depression of the sternum, leading to bulging at the costochondral junctions (thus named *rosary*), which can be depicted on chest radiographs (54,55). Similar findings may be seen in Menkes syndrome, as the disorder is complicated by impairment of collagen biosynthesis due to copper deficiency.

The finding of rachitic rosary in rickets reflects abundant undermineralized osteoid matrix at the chondro-osseous junction (Fig 21) (56). Metabolic bone disease of prematurity is commonly seen in premature infants, representing the combination of rickets and osteoporosis, and may be associated with rosary (57). The diagnosis is usually straightforward based on the patient's history.

Although less frequent, nonaccidental injury can cause fractures of the costochondral junction that may manifest as imaging findings that resemble a rachitic rosary. This type of injury is an equivalent of the classic metaphyseal lesion

Table 4: Diffuse Rib Abnormalities

Entity	Imaging Findings	Notes
Thin ribs with fractures		
Osteogenesis imperfecta	Slim bones with osteoporosis	Largely related to type 1 collagen abnormalities (*COL1A1* and *COL1A2* mutations)
Neonatal hyperparathyroidism	Slim bones with coarse trabeculae and metaphyseal subperiosteal resorption	Caused by abnormal sensing of calcium or impaired placental calcium transport
Hypophosphatasia	Slim bones with defective ossification of bone ends	Impaired bone mineralization due to defective alkaline phosphatase
Thin ribs without fractures		
Myotonic dystrophy	Slimness of ribs disproportional to the long bones	A consequence of fetal hypokinesia
Severe myopathy, spinal muscular atrophy	Slimness of ribs proportional to the long bones	A consequence of fetal hypokinesia
Arthrogryposis	Variable degrees of slimness	A heterogeneous group of congenital joint contracture
Potter sequence	Slimness of ribs associated with hypoplastic lung	A consequence of intrauterine constraint
Campomelic dysplasia	Thin ribs with characteristic scapular hypoplasia	Associated with bowed limbs; sex reversal in patients with chromosome XY
Thick and/or dense ribs		
Bone marrow hyperplasia	Diffusely thick ribs with coarse trabeculae	Most commonly associated with hereditary hemolytic anemia
Mucopolysaccharidosis	Thickening of the anterior and middle ribs (oar-like ribs)	Associated with distinctive skeletal changes termed *dysostosis multiplex*
Short ribs		
Skeletal ciliopathies	Horizontally-oriented short ribs	A group of disorders due to abnormal biogenesis of primary cilia
Other characteristic rib shapes		
Paternal uniparental disomy 14	Coat-hanger ribs	Caused by abnormal imprinting of genes in chromosome 14
Melnick-Needles syndrome, frontometaphyseal dysplasia	Ribbonlike distorted ribs	Bone dysplasias due to abnormalities of a cytoskeletal protein (*FLNA* mutations)

most often detected in the long bones. In general, these lesions are more difficult to discern in the ribs due to the shape of the ribs and relatively diminished healing callus formation but may manifest as areas of focal swelling in the anterior thorax.

Diffuse Rib Abnormalities

Diffuse rib abnormalities are usually apparent in the neonatal period and categorized based on the nature of the morphologic abnormalities, such as thin ribs (without and with fractures), thick ribs, and short ribs (Table 4). These diffuse rib abnormalities are typically part of a broader constitutional skeletal disorder (eg, chromosome aberration, metabolic disorders, malformation syndromes, and bone dysplasias), neuromuscular disorder, or connective tissue disorder and are associated with abnormalities in other bones. There are few diffuse rib abnormalities that are disease specific (although not 100% pathognomonic), including coat hanger ribs, diffusely twisted ribs, and rib gaps.

Thin Ribs with Fractures

A combination of thin ribs and multifocal rib fractures is suggestive of brittle bone disorders and generalized osteoporosis. These conditions are caused by decreased bone formation and/or increased bone resorption. The long bones are slender or overconstricted.

Osteogenesis imperfecta is the representative brittle bone disorder, with most cases caused by abnormal type I collagen (*COL1A1* or *COL1A2* mutations) that impair intramembranous bone formation (58). Radiographic findings include diffusely slender bones (including ribs) with diffuse osteoporosis and multiple fractures, delayed ossification of the skull, and presence of wormian bones (Fig 22). Severely affected patients may present with thick beaded ribs as a consequence of remodeling of multiple recurrent fractures in utero (59).

Other brittle bone disorders include neonatal hyperparathyroidism and hypophosphatasia. Neonatal hyperparathyroidism is accompanied by subperiosteal bone resorption of the metaphyses (Fig 23) (60). Hypophosphatasia manifests with a tonguelike ossification defect of the metaphyses. These metaphyseal changes can be seen in the proximal humerus on chest radiographs, which allows differentiation from osteogenesis imperfecta (61).

Thin Ribs without Fracture

Lack of normal fetal movement from any cause (eg, congenital neuromuscular disorders, intrauterine joint contracture, and intrauterine constraint) hampers normal skeletal development

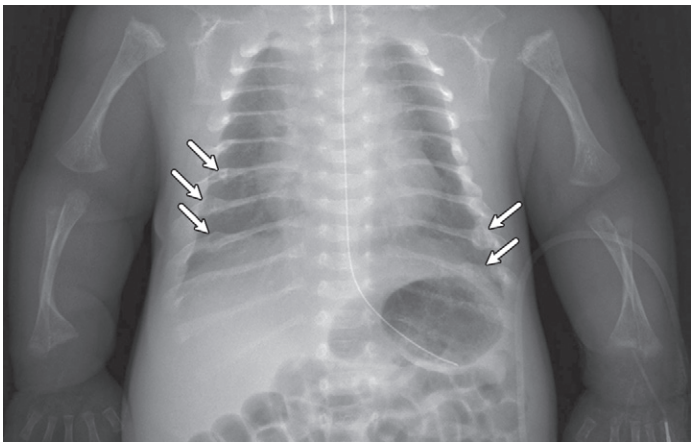

Figure 22. Diffusely thin ribs with fractures in a neonate with osteogenesis imperfecta. Frontal chest radiograph shows osteoporotic, diffusely thin, deformed ribs as a result of multiple fractures (arrows). The bilateral proximal humeri are osteoporotic with irregular proximal metaphyses. The vertebral bodies are compressed.

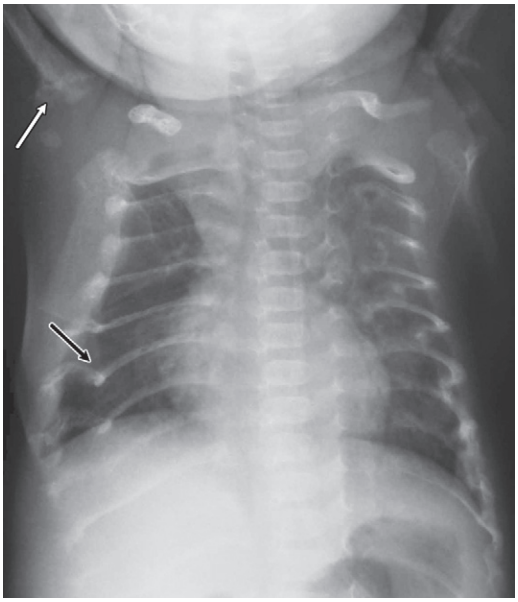

Figure 23. Diffusely thin ribs with fractures in a neonate with hyperparathyroidism. Frontal chest radiograph shows diffusely thin ribs with multiple fractures (black arrow) and deformities as well as subperiosteal resorption of the proximal humeri (white arrow).

Figure 24. Diffusely thin ribs without fractures in a neonate with myotonic dystrophy. Frontal chest radiograph shows extremely thin ribs that are out of proportion to the width of the right humerus. The mineralization is normal, and osteoporosis is not present.

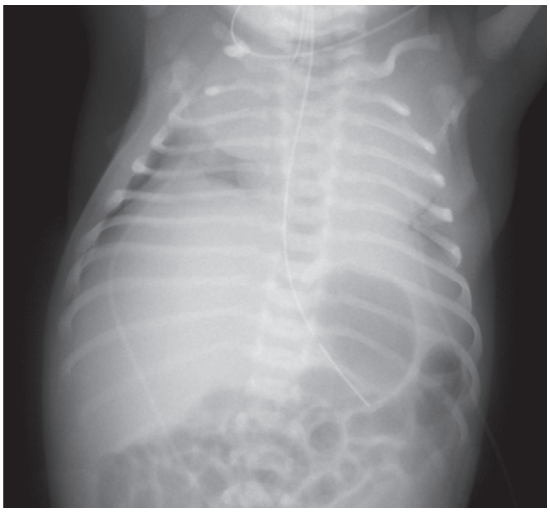

Figure 25. Diffusely thin ribs without fractures in a neonate with Potter sequence. Frontal chest radiograph shows diffusely thin ribs with poorly expanded hypoplastic lungs, complicated by right lateral pneumothorax. Abdominal US findings (not shown) revealed bilateral enlarged echogenic kidneys consistent with autosomal recessive polycystic kidney disease.

and results in overtubulation (slenderness) of long bones and ribs. However, these gracile bones are not brittle, contrasting with thin and fragile bones seen in osteogenesis imperfecta and metabolic bone diseases.

Gracile ribs are common in severe neuromuscular disorders, such as spinal muscular atrophy, congenital myopathy, and myotonic dystrophy. Neonates with these disorders usually show severe hypotonia and less commonly present with congenital joint contractures. Characteristically, the ribs in myotonic dystrophy tend to be disproportionately slender to the long bones as compared to those in patients with spinal muscular atrophy and congenital myopathy (Fig 24). Severe oligohydramnios restricts fetal movement, leading to joint contractures and pulmonary hypoplasia associated with gracile long bones and slim ribs. Potter sequence, characterized by oliguria, oligohydramnios, lung hypoplasia, and positional deformities due to bilateral renal dysplasia, is the most severe condition in this category (Fig 25). In some cases of multiple gestation, intrauterine constraint may cause thin ribs.

Other conditions with thin ribs include trisomy 18 syndrome (also with narrow ilia), campomelic dysplasia (with scapular hypoplasia), infantile Marfan syndrome (with arachnodactyly), and Antley-Bixler syndrome (with arachnodactyly, joint ankylosis, and craniosynostosis).

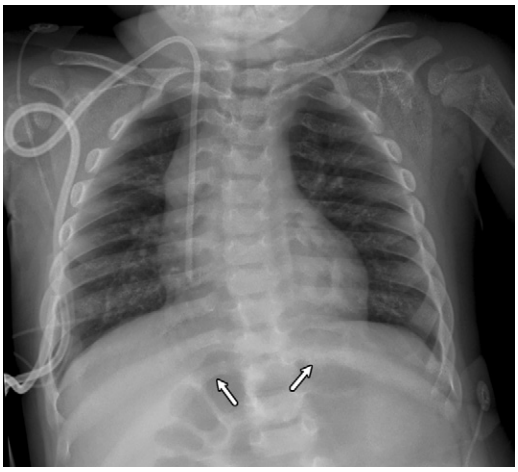

Figure 26. Thick ribs in a 5-year-old girl with Hurler syndrome. Frontal chest radiograph shows widening of the posterior ribs. The costal end of the inferior ribs is constricted (arrows), giving rise to a canoe-paddle appearance characteristic of mucopolysaccharidoses. A central venous catheter is in place for enzyme replacement therapy.

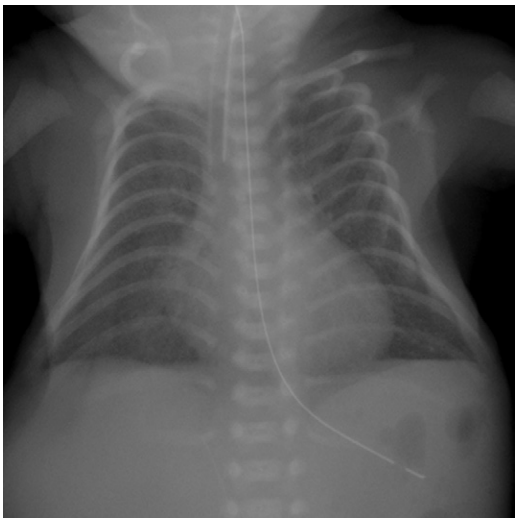

Figure 28. Coat-hanger ribs in a neonate with paternal uniparental disomy 14. Frontal chest radiograph shows a bell-shaped thorax with cranially directed posterior ribs and caudally directed anterior ribs, resulting in a coat-hanger appearance.

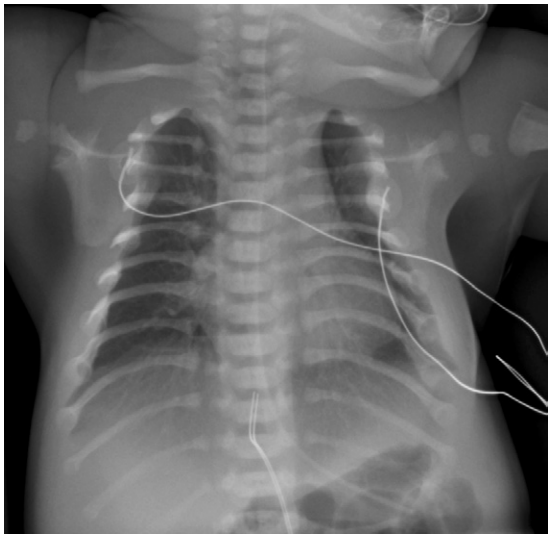

Figure 27. Short ribs in a neonate with Jeune asphyxiating thoracic dysplasia. Frontal chest radiograph shows markedly short and horizontally oriented ribs. The clavicles are high in position, and premature ossification of the proximal humeral epiphyses is seen.

Thick and/or Dense Ribs

The ribs can be broadened or thickened as a result of expansion of the medullary cavity or abnormal modeling of the metadiaphysis. Expansion of the medullary cavity can be seen in patients with chronic bone marrow hyperplasia (eg, thalassemia), storage diseases (eg, mucopolysaccharidosis), and juvenile Paget disease, while abnormal metadiaphyseal modeling can be seen in a variety of sclerosing bone dysplasias.

Chronic hematopoietic bone marrow hyperplasia expands the medullary space and distorts the trabeculae, leading to thick ribs with a coarse trabecular pattern (62). Mucopolysaccharidosis shows expansion of the anterior and middle segments of the ribs but constriction of the posterior end of the ribs (termed *oarlike ribs* or *canoe-paddle ribs*) (Fig 26) (59). Juvenile Paget disease shows severe expansion of the ribs and tubular bones due to abnormally increased endosteal bone resorption (63).

Sclerosing bone dysplasias encompass a heterogeneous group of disorders due to either increased bone formation (eg, Camurati-Engelmann disease, Pyle disease, and craniometaphyseal dysplasia) or decreased bone resorption (eg, osteopetrosis and pyknodysostosis). The latter group shows generalized osteosclerosis and dense ribs because decreased bone resorption causes abundant immature bones. The bones are dense but brittle and are prone to fractures (64).

Short Ribs

Severe shortening of the ribs is associated with thoracic and pulmonary hypoplasia, which leads clinically to respiratory failure. Severe thoracic hypoplasia is a hallmark of skeletal ciliopathies, a group of bone dysplasias associated with abnormalities of the primary cilia, including Jeune asphyxiating thoracic dysplasia (Fig 27) and Ellis–van Creveld syndrome (65). The extremely short ribs tend to be horizontally oriented. The horizontal ribs cause a cephalad position of the sternum and clavicles, leading to high-positioned (handlebar-like) clavicles. Other bone dysplasias with a narrow thorax include thanatophoric dysplasia, Shwachman-Bodian-Diamond syndrome, and metatropic dysplasia.

Coat-Hanger Ribs

A sharp apex-superior angulation of the posterior segment of the ribs gives a coat-hanger appearance, a rare but characteristic finding seen in only a few disorders. The finding is classically seen in paternal uniparental disomy 14 (Kagami-Ogata syndrome) (66,67), which is also associated with characteristic facial features, polyhydramnios, omphalocele and/or hypoplasia of the abdominal musculatures, and hepatoblastoma in less than 10% of cases (Fig 28) (66). The coat-hanger–shaped ribs

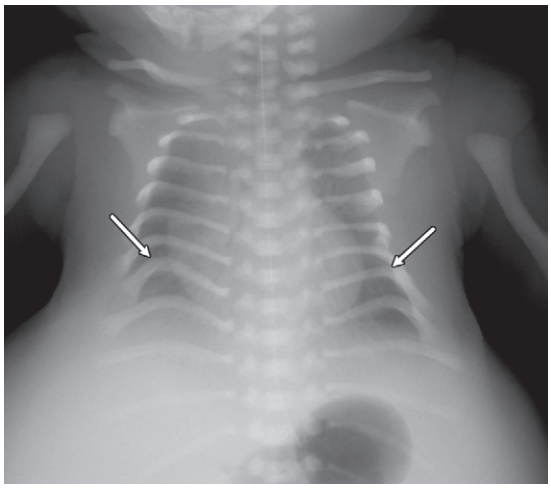

Figure 29. Coat-hanger ribs in a neonate with Sensenbrenner syndrome. Frontal chest radiograph shows coat-hanger–appearing ribs in the midlevel ribs (arrows). The upper and lower ribs are relatively normal, as opposed to diffusely abnormal ribs seen in paternal uniparental disomy 14.

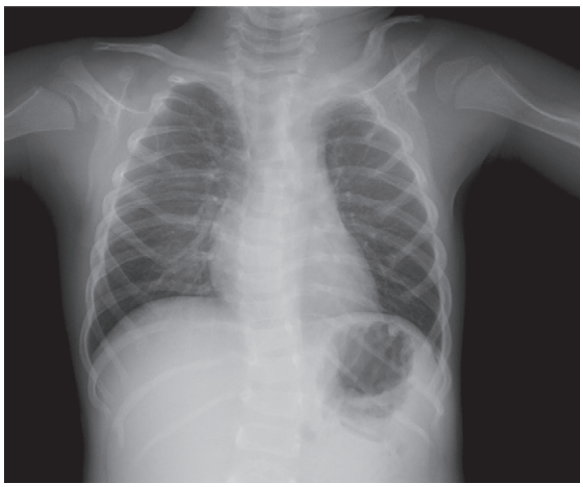

Figure 30. Diffusely twisted ribs in a child with Melnick-Needles syndrome. Frontal chest radiograph shows thinning and scalloping of all ribs, giving rise to a ribbonlike appearance. Metaphyseal broadening and constriction of the metadiaphyseal junction of the proximal humeri and hypoplasia of the distal clavicle are also noted.

are more diagnostic of this disorder than the other findings. Coat-hanger ribs may also be seen in a subset of patients with Sensenbrenner syndrome, one of the skeletal ciliopathies in which only the middle and lower ribs are affected (Fig 29).

Diffusely Twisted Ribs

Twisted ribs are usually localized in patients with NF1, whereas generalized rib twisting is present in bone dysplasias caused by abnormalities in the *filamin A* gene including Melnick-Needles syndrome and frontometaphyseal dysplasia. Irregular costal contours tend to be especially conspicuous in patients with Melnick-Needles syndrome, whose severely distorted ribs are called ribbon ribs (Fig 30) (68).

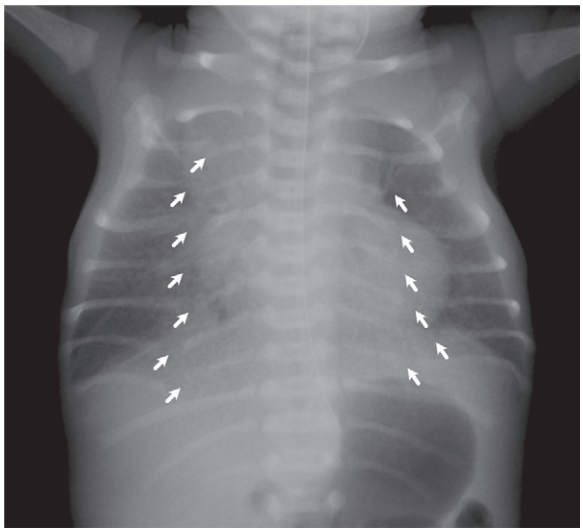

Figure 31. Rib gaps in a neonate with cerebro-costo-mandibular syndrome. Frontal chest radiograph shows multiple posterior bilateral rib gaps (arrows).

Rib Gaps

Rib gaps refer to multiple bone defects in the posterior ribs. The costal malformation is a characteristic finding of cerebrocostomandibular syndrome, a malformation syndrome characterized by distinctive rib anomalies with a narrow thorax and micrognathia (Fig 31). The pathogenesis is maldevelopment of the posterior segment and posterolateral arc of the rib. A reduced number of ribs and abnormal costotransverse articulation may also be found (69).

Conclusion

The ribs are imaged in all chest radiographs. Rib abnormalities may be present even when no osseous condition is suspected, which may provide a clue to underlying conditions such as those described in this article. Performing a vigilant search for rib abnormalities on every chest radiograph is essential, as incidental rib lesions are not uncommon and may have important clinical implications. Recognizing specific patterns of disease will help the radiologist correctly ascertain the nature of the lesion and direct appropriate management. Cross-sectional imaging may still be required, especially for tumors and tumorlike lesions and infectious and inflammatory conditions.

Author affiliations.—From the Department of Radiology, Keio University School of Medicine, Tokyo, Japan (Y.T., T.N., M.J.); Department of Radiology, Tokyo Metropolitan Children's Medical Center, Tokyo, Japan (Y.T., T.K.); Department of Radiology, Boston Children's Hospital and Harvard Medical School, 300 Longwood Ave, Boston, MA 02115 (A.H., S.D.B.); Department of Radiology, Musashino-Yowakai Hospital, Tokyo, Japan (G.N.); and Department of Radiology, National Center for Child Health and Development, Tokyo, Japan (O.M.). Presented as an education exhibit at the 2022 RSNA Annual Meeting. Received April 3, 2023; revision requested June 13 and received June 21; accepted June 23. **Address correspondence to A.H.** (email: *atsuhiko.handa@childrens.harvard.edu*).

Disclosures of conflicts of interest.—All authors, the editor, and the reviewers have disclosed no relevant relationships.

References

1. Glass RB, Norton KI, Mitre SA, Kang E. Pediatric ribs: a spectrum of abnormalities. RadioGraphics 2002;22(1):87–104.

2. Huang R, Zhi Q, Schmidt C, Wilting J, Brand-Saberi B, Christ B. Sclerotomal origin of the ribs. Development 2000;127(3):527–532.
3. Aoyama H, Mizutani-koseki S, Koseki H. Three developmental compartments involved in rib formation. Int J Dev Biol 2005;49(2-3):325–333.
4. Aboughalia HA, Ngo AV, Menashe SJ, Kim HHR, Iyer RS. Pediatric rib pathologies: clinicoimaging scenarios and approach to diagnosis. Pediatr Radiol 2021;51(10):1783–1797.
5. Moser RP Jr, Davis MJ, Gilkey FW, et al. Primary Ewing sarcoma of rib. RadioGraphics 1990;10(5):899–914.
6. Murphey MD, Choi JJ, Kransdorf MJ, Flemming DJ, Gannon FH. Imaging of osteochondroma: variants and complications with radiologic-pathologic correlation. RadioGraphics 2000;20(5):1407–1434.
7. Baez JC, Lee EY, Restrepo R, Eisenberg RL. Chest wall lesions in children. AJR Am J Roentgenol 2013;200(5):W402–W419.
8. Patel M, Bauer TW, Santoscoy T, Ilaslan H. Osteochondroma of the fifth rib resulting in recurrent hemothorax. Skeletal Radiol 2015;44(12):1853–1856.
9. Hughes EK, James SL, Butt S, Davies AM, Saifuddin A. Benign primary tumours of the ribs. Clin Radiol 2006;61(4):314–322.
10. Kim S, Lee S, Arsenault DA, Strijbosch RA, Shamberger RC, Puder M. Pediatric rib lesions: a 13-year experience. J Pediatr Surg 2008;43(10):1781–1785.
11. Soyer T, Karnak I, Talim B, Tanyel FC. Aneurysmal bone cyst of the rib in a child: report of a case. Surg Today 2005;35(10):886–889.
12. Sabanathan S, Chen K, Robertson CS, Salama FD. Aneurysmal bone cyst of the rib. Thorax 1984;39(2):125–130.
13. Mahalingam H, Ramasundaram M, Rajendiran S, Jayaraman D. Mesenchymal Hamartoma of the Chest Wall in an Infant - A Benign Entity Masquerading as Malignancy. J Indian Assoc Pediatr Surg 2021;26(3):184–187.
14. Groom KR, Murphey MD, Howard LM, Lonergan GJ, Rosado-De-Christenson ML, Torop AH. Mesenchymal hamartoma of the chest wall: radiologic manifestations with emphasis on cross-sectional imaging and histopathologic comparison. Radiology 2002;222(1):205–211.
15. Wang MX, Segaran N, Bhalla S, et al. Tuberous Sclerosis: Current Update. RadioGraphics 2021;41(7):1992–2010.
16. Avila NA, Dwyer AJ, Rabel A, Darling T, Hong CH, Moss J. CT of sclerotic bone lesions: imaging features differentiating tuberous sclerosis complex with lymphangioleiomyomatosis from sporadic lymphangioleiomyomatosis. Radiology 2010;254(3):851–857.
17. Boronat S, Barber I, Thiele EA. Sclerotic bone lesions in tuberous sclerosis complex: A genotype-phenotype study. Am J Med Genet A 2017;173(7):1891–1895.
18. Li P, Boronat S, Geffrey AL, Barber I, Grottkau BE, Thiele EA. Rib and vertebral bone fibrous dysplasia in a child with tuberous sclerosis complex. Am J Med Genet A 2015;167A(11):2755–2757.
19. Murphey MD, Senchak LT, Mambalam PK, Logie CI, Klassen-Fischer MK, Kransdorf MJ. From the radiologic pathology archives: ewing sarcoma family of tumors: radiologic-pathologic correlation. RadioGraphics 2013;33(3):803–831.
20. Nam SJ, Kim S, Lim BJ, et al. Imaging of primary chest wall tumors with radiologic-pathologic correlation. RadioGraphics 2011;31(3):749–770.
21. Yaman Bajin İ, Kurucu N, Oğuz B, et al. Primary Osteosarcoma of the Rib: A Case Report and Review of the Literature. J Pediatr Hematol Oncol 2018;40(1):48–50.
22. Tateishi U, Gladish GW, Kusumoto M, et al. Chest wall tumors: radiologic findings and pathologic correlation: part 2. Malignant tumors. RadioGraphics 2003;23(6):1491–1508.
23. Sundaram M, McGuire MH, Herbold DR. Magnetic resonance imaging of osteosarcoma. Skeletal Radiol 1987;16(1):23–29.
24. Sato TS, Handa A, Priya S, Watal P, Becker RM, Sato Y. Neurocristopathies: Enigmatic Appearances of Neural Crest Cell-derived Abnormalities. RadioGraphics 2019;39(7):2085–2102.
25. Suita S, Tajiri T, Sera Y, et al. The characteristics of mediastinal neuroblastoma. Eur J Pediatr Surg 2000;10(6):353–359.
26. McElroy KM, Binkovitz LA, Trout AT, et al. Pediatric applications of Dotatate: early diagnostic and therapeutic experience. Pediatr Radiol 2020;50(7):882–897.
27. Maruyama D, Watanabe T, Beppu Y, et al. Primary bone lymphoma: a new and detailed characterization of 28 patients in a single-institution study. Jpn J Clin Oncol 2007;37(3):216–223.
28. Mulligan ME, McRae GA, Murphey MD. Imaging features of primary lymphoma of bone. AJR Am J Roentgenol 1999;173(6):1691–1697.
29. Egeler RM, D'Angio GJ. Langerhans cell histiocytosis. J Pediatr 1995;127(1):1–11.
30. Zaveri J, La Q, Yarmish G, Neuman J. More than just Langerhans cell histiocytosis: a radiologic review of histiocytic disorders. RadioGraphics 2014;34(7):2008–2024.
31. Monsereenusorn C, Rodriguez-Galindo C. Clinical Characteristics and Treatment of Langerhans Cell Histiocytosis. Hematol Oncol Clin North Am 2015;29(5):853–873.
32. Azouz EM, Saigal G, Rodriguez MM, Podda A. Langerhans' cell histiocytosis: pathology, imaging and treatment of skeletal involvement. Pediatr Radiol 2005;35(2):103–115.
33. Peltola H, Pääkkönen M. Acute osteomyelitis in children. N Engl J Med 2014;370(4):352–360.
34. Crone AM, Wanner MR, Cooper ML, Fox TG, Jennings SG, Karmazyn B. Osteomyelitis of the ribs in children: a rare and potentially challenging diagnosis. Pediatr Radiol 2020;50(1):68–74.
35. Gensure RC, Mäkitie O, Barclay C, et al. A novel COL1A1 mutation in infantile cortical hyperostosis (Caffey disease) expands the spectrum of collagen-related disorders. J Clin Invest 2005;115(5):1250–1257.
36. Nistala H, Mäkitie O, Jüppner H. Caffey disease: new perspectives on old questions. Bone 2014;60:246–251.
37. Sanders DG, Weijers RE. MRI findings in Caffey's disease. Pediatr Radiol 1994;24(5):325–327.
38. Woo K, Emery J, Peabody J. Cortical hyperostosis: a complication of prolonged prostaglandin infusion in infants awaiting cardiac transplantation. Pediatrics 1994;93(3):417–420.
39. Gardiner JS, Zauk AM, Donchey SS, McInerney VK. Prostaglandin-induced cortical hyperostosis. Case report and review of the literature. J Bone Joint Surg Am 1995;77(6):932–936.
40. Moreno-Mateo F, Perea SH, Onel KB. Chronic recurrent multifocal osteomyelitis: diagnosis and treatment. Curr Opin Pediatr 2021;33(1):90–96.
41. Navallas M, Inarejos Clemente EJ, Iglesias E, Rebollo-Polo M, Hernández JC, Navarro OM. Autoinflammatory diseases in childhood, part 2: polygenic syndromes. Pediatr Radiol 2020;50(3):431–444.
42. Buch K, Thuesen ACB, Brøns C, Schwarz P. Chronic Non-bacterial Osteomyelitis: A Review. Calcif Tissue Int 2019;104(5):544–553.
43. Khanna G, Sato TS, Ferguson P. Imaging of chronic recurrent multifocal osteomyelitis. RadioGraphics 2009;29(4):1159–1177.
44. Roderick MR, Shah R, Rogers V, Finn A, Ramanan AV. Chronic recurrent multifocal osteomyelitis (CRMO) - advancing the diagnosis. Pediatr Rheumatol Online J 2016;14(1):47.
45. Jansson A, Renner ED, Ramser J, et al. Classification of non-bacterial osteitis: retrospective study of clinical, immunological and genetic aspects in 89 patients. Rheumatology (Oxford) 2007;46(1):154–160.
46. Patel NB, Stacy GS. Musculoskeletal manifestations of neurofibromatosis type 1. AJR Am J Roentgenol 2012;199(1):W99–W106.
47. Lala S, Mulliken JB, Alomari AI, Fishman SJ, Kozakewich HP, Chaudry G. Gorham-Stout disease and generalized lymphatic anomaly--clinical, radiologic, and histologic differentiation. Skeletal Radiol 2013;42(7):917–924.
48. Ruggieri P, Montalti M, Angelini A, Alberghini M, Mercuri M. Gorham-Stout disease: the experience of the Rizzoli Institute and review of the literature. Skeletal Radiol 2011;40(11):1391–1397.
49. Ozeki M, Fujino A, Matsuoka K, Nosaka S, Kuroda T, Fukao T. Clinical Features and Prognosis of Generalized Lymphatic Anomaly, Kaposiform Lymphangiomatosis, and Gorham-Stout Disease. Pediatr Blood Cancer 2016;63(5):832–838.
50. Carty H, Pierce A. Non-accidental injury: a retrospective analysis of a large cohort. Eur Radiol 2002;12(12):2919–2925.
51. Barsness KA, Cha ES, Bensard DD, et al. The positive predictive value of rib fractures as an indicator of nonaccidental trauma in children. J Trauma 2003;54(6):1107–1110.
52. Ng CS, Hall CM. Costochondral junction fractures and intra-abdominal trauma in non-accidental injury (child abuse). Pediatr Radiol 1998;28(9):671–676.
53. Kleinman PK, Marks SC Jr, Nimkin K, Rayder SM, Kessler SC. Rib fractures in 31 abused infants: postmortem radiologic-histopathologic study. Radiology 1996;200(3):807–810.
54. Chang CY, Rosenthal DI, Mitchell DM, Handa A, Kattapuram SV, Huang AJ. Imaging Findings of Metabolic Bone Disease. RadioGraphics 2016;36(6):1871–1887.
55. Narchi H, Thomas M. A painful limp. J Paediatr Child Health 2000;36(3):277–278.
56. Shore RM, Chesney RW. Rickets: Part II. Pediatr Radiol 2013;43(2):152–172.
57. Servaes S, States L, Wood J, Schilling S, Christian CW. Rachitic change and vitamin D status in young children with fractures. Skeletal Radiol 2020;49(1):85–91 [Published correction appears in Skeletal Radiol 2020;49:341.]
58. Forlino A, Marini JC. Osteogenesis imperfecta. Lancet 2016;387(10028):1657–1671.
59. Handa A, Nishimura G, Zhan MX, Bennett DL, El-Khoury GY. A primer on skeletal dysplasias. Jpn J Radiol 2022;40(3):245–261.

60. Nguyen VC, Sennott WM, Knox GS. Neonatal hyperparathyroidism. Radiology 1974;112(1):175–176.
61. Offiah AC, Vockley J, Munns CF, Murotsuki J. Differential diagnosis of perinatal hypophosphatasia: radiologic perspectives. Pediatr Radiol 2019;49(1):3–22.
62. Hajimoradi M, Haseli S, Abadi A, Chalian M. Musculoskeletal imaging manifestations of beta-thalassemia. Skeletal Radiol 2021;50(9):1749–1762.
63. Polyzos SA, Cundy T, Mantzoros CS. Juvenile Paget disease. Metabolism 2018;80:15–26.
64. Ihde LL, Forrester DM, Gottsegen CJ, et al. Sclerosing bone dysplasias: review and differentiation from other causes of osteosclerosis. RadioGraphics 2011;31(7):1865–1882.
65. Handa A, Voss U, Hammarsjö A, Grigelioniene G, Nishimura G. Skeletal ciliopathies: a pattern recognition approach. Jpn J Radiol 2020;38(3):193–206.
66. Kagami M, Kurosawa K, Miyazaki O, Ishino F, Matsuoka K, Ogata T. Comprehensive clinical studies in 34 patients with molecularly defined UPD(14)pat and related conditions (Kagami-Ogata syndrome). Eur J Hum Genet 2015;23(11):1488–1498.
67. Miyazaki O, Nishimura G, Kagami M, Ogata T. Radiological evaluation of dysmorphic thorax of paternal uniparental disomy 14. Pediatr Radiol 2011;41(8):1013–1019.
68. Coste F, Maroteaux P, Chouraki L. Osteodysplasty (Melnick and Needles syndrome). Report of a case. Ann Rheum Dis 1968;27(4):360–366.
69. Tooley M, Lynch D, Bernier F, et al. Cerebro-costo-mandibular syndrome: Clinical, radiological, and genetic findings. Am J Med Genet A 2016;170A(5):1115–1126.